

**THE APPLICATION OF PIEZOCERAMIC BENDER ELEMENTS TO
THE LABORATORY MEASUREMENT OF ELASTIC WAVE
VELOCITIES**

By

Kevin Donald Gibson Jarvis

B. Eng., University of Saskatchewan, 1986

A THESIS SUBMITTED IN PARTIAL FULFILLMENT OF
THE REQUIREMENTS FOR THE DEGREE OF
MASTER OF SCIENCE

in

THE FACULTY OF GRADUATE STUDIES
(Department of Geophysics and Astronomy)

We accept this thesis as conforming
to the required standard

THE UNIVERSITY OF BRITISH COLUMBIA

November 1994

© Kevin Donald Gibson Jarvis, 1994

In presenting this thesis in partial fulfilment of the requirements for an advanced degree at the University of British Columbia, I agree that the Library shall make it freely available for reference and study. I further agree that permission for extensive copying of this thesis for scholarly purposes may be granted by the head of my department or by his or her representatives. It is understood that copying or publication of this thesis for financial gain shall not be allowed without my written permission.

Department of GEOPHYSICS & ASTRONOMY

The University of British Columbia
Vancouver, Canada

Date 94-12-02

ABSTRACT

The objective of this thesis is to evaluate bender elements as a source and receiver of elastic waves in cohesionless sand. The techniques used to build the benders that are detailed include the use of an impedance analyzer to monitor changes in the electrical and mechanical response. Placing the benders in a bucket of sand demonstrated the short compact nature of the bender waveform in both a shear and compressional wave orientation. An experiment in a non-homogeneous sandbox showed the change in shear waveform with separation of the elements. A Plexiglas cylinder with benders was used to measure changes in shear and compressional wave velocity as a function of confining pressure and the saturation with water and silicon oil. The effects of friction along the walls of the cylinder resulted in an unknown and irreproducible confining stress on the sand between the benders. An experiment to study the effect of silicon oil viscosity on shear modulus was inconclusive as a result of the unknown stress condition. The bender elements proved to be an excellent source and receiver of elastic waves in cohesionless sand.

TABLE OF CONTENTS

ABSTRACT.....	ii
TABLE OF CONTENTS.....	iii
LIST OF FIGURES	v
ACKNOWLEDGMENTS	viii
Chapter 1: INTRODUCTION.....	1
Chapter 2: BENDER ELEMENTS.....	4
2.1 Introduction.....	4
2.2 Bender Element Description	5
2.3 Experimental Procedures	7
2.3.1 Bender Building	7
2.3.2 Sand Bucket Experiments	16
2.3.3 Sandbox Experiments	19
2.4 Discussion and Results.....	21
2.4.1 Benders as a Source of Shear Waves	22
2.4.2 Benders as a Source of Compressional Waves	25
2.4.3 Sandbox Bender Experiment	28
2.5 Summary	32

Chapter 3: THE MEASUREMENT OF VELOCITIES IN A COHESIONLESS SAND PACK USING A CONFINING PRESSURE CELL	33
3.1 Introduction	33
3.2 The Effect of Fluid Viscosity on Elastic Wave Velocities	35
3.3 The Stress State of a Sand Pack Under Uniaxial Compression	39
3.4 The Effect of Water Saturation on a Sand Pack Under Uniaxial Load.....	41
3.5 Experimental Procedures	43
3.5.1 Apparatus Description.....	43
3.5.2 Measurement Procedure.....	45
3.6 Discussion and Results.....	48
3.6.1 Compressional Waves in Distilled Water	49
3.6.2 Water Saturation Experiments	51
3.6.3 Silicon Oil Saturation Experiments.....	60
3.6.3.1 10 mm ² /s Saturation Experiment	62
3.6.3.2 100 mm ² /s Saturation Experiment	62
3.6.3.3 1000 mm ² /s Saturation Experiment	65
3.6.3.4 10 000 mm ² /s Saturation Experiment	65
3.6.3.5 Discussion of Silicon Oil Experiments	67
3.7 Summary	72
Chapter 4: CONCLUSIONS	73
REFERENCES	75

LIST OF FIGURES

2.1	Diagram of piezoceramic bender element	6
2.2	Admittance graphs of blue bender with leads attached.....	9
2.3	Admittance graphs of green bender with leads attached.....	9
2.4	Admittance graphs of blue bender with Plexiglas base attached	10
2.5	Admittance graphs of green bender with Plexiglas base attached	10
2.6	Admittance graphs of blue bender with one coat of Sun Cure epoxy.....	12
2.7	Admittance graphs of green bender with one coat of Sun Cure epoxy.....	12
2.8	Admittance graphs of blue bender with Swagelok tubing and epoxy coating	13
2.9	Admittance graphs of green bender with Swagelok tubing and epoxy coating..	13
2.10	Admittance graphs of blue bender after final coating of epoxy	14
2.11	Admittance graphs of green bender after final coating of epoxy	14
2.12	Admittance graphs of blue bender in contact with a sand pack.....	15
2.13	Admittance graphs of green bender in contact with a sand pack.....	15
2.14	Admittance graphs of bender #1	17
2.15	Admittance graphs of bender #2	17
2.16	Diagram of the sandbox experiment	20
2.17a	Shear waveform from the sand bucket experiment.....	23
2.17b	Amplitude spectrum of shear waveform from sand bucket experiment	23
2.18	Diagram illustrating the variation in shear waveform with input voltage	24
2.19	Graph of the first peak amplitude as a function of input sq. wave voltage.....	26
2.20	Graph of the first trough amplitude as a function of input sq. wave voltage.....	27
2.21a	Compressional waveform from the sand bucket experiment.....	29
2.21b	Amp. spectrum of compressional waveform from sand bucket experiment.....	29
2.22	Sandbox data	30

3.1	Diagram showing the crack-like porosity in a packing of spherical grains	36
3.2	P-wave and S-wave velocity as a function of frequency and viscosity for Navajo sandstone	38
3.3	P-wave velocity as a function of frequency and viscosity for glass beads	38
3.4	Diagram showing the force balance on a cylinder under uniaxial compression.	40
3.5	Diagram of the confining pressure cell with loading and saturating apparatus ..	44
3.6a	Waveform from confining pressure cell with distilled water	50
3.6b	Amplitude spectrum of distilled water waveform.....	50
3.7	Graph of P-wave velocity in distilled water as a function of water temp.	51
3.8a	Shear waveform in sand pack before saturation with water	53
3.8b	Shear waveform in sand pack after saturation with water	53
3.9a	Shear wave velocity as a function of axial stress for a dry and water saturated sand pack.....	54
3.9b	Shear modulus as a function of axial stress for a dry and water saturated sand pack.....	54
3.10a	Compressional waveform in sand pack before saturation with water	57
3.10b	Compressional waveform in sand pack after saturation with water	57
3.11a	Compressional wave velocity as a function of axial stress for a dry and water saturated sand pack	59
3.11b	Uniaxial strain modulus as a function of axial stress for a dry and water saturated sand pack	59
3.12a	Shear waveform in sand pack before saturation with 100 mm ² /s silicon oil	61
3.12b	Shear waveform in sand pack after saturation with 100 mm ² /s silicon oil	61
3.13a	Shear wave velocity as a function of axial stress for a dry and 10 mm ² /s saturated sand pack	63
3.13b	Shear modulus as a function of axial stress for a dry and 10 mm ² /s saturated sand pack	63

3.14a	Shear wave velocity as a function of axial stress for a dry and 100 mm ² /s saturated sand pack	64
3.14b	Shear modulus as a function of axial stress for a dry and 100 mm ² /s saturated sand pack	64
3.15a	Shear wave velocity as a function of axial stress for a dry and 1000 mm ² /s saturated sand pack	66
3.15b	Shear modulus as a function of axial stress for a dry and 1000 mm ² /s saturated sand pack	66
3.16a	Shear wave velocity as a function of axial stress for a dry and 10 000 mm ² /s saturated sand pack	68
3.16b	Shear modulus as a function of axial stress for a dry and 10 000 mm ² /s saturated sand pack	68
3.17	Shear modulus at 50 kPa axial stress as a function of viscosity	70
3.18	Shear modulus at 200 kPa axial stress as a function of viscosity	70
3.19	Shear modulus ratios at 50 kPa axial stress as a function of viscosity	71
3.20	Shear modulus ratios at 200 kPa axial stress as a function of viscosity	71

ACKNOWLEDGMENTS

I would like to express my gratitude to the entire Rock Physics Research Group at UBC for providing ideas and encouragement throughout the duration of my thesis. In particular, my advisor, Rosemary Knight provided continuous encouragement and support for the final data interpretation and the continuous cell design revisions which were made to obtain reasonable data. The experimental experience of Dave Butler resulted in many ideas which were crucial to the final design of the apparatus. I would also like to express my thanks to Scott Jackson in the Department of Civil Engineering at UBC who provided the raw bender elements and the original bender design procedures. Without the bender elements the research in this thesis would not have been possible.

This research was supported by funding to Rosemary Knight from the Natural Sciences and Engineering Research Council. The author was personally supported by a Natural Sciences and Engineering Research Council postgraduate scholarship (PGX 1).

Chapter 1

INTRODUCTION

Seismic techniques provide remote, non-destructive methods for monitoring subsurface properties. The oil exploration industry has developed a variety of seismic techniques which are extremely useful for examining changes in the subsurface at great depth (km). The wavelengths of the seismic waves which propagate to such depths are typically 50 to 100 m. It is the wavelength of the propagating seismic energy which determines the resolution. A 50 to 100 m wavelength is approximately the thickness of the geologic formations of interest, that act as reservoirs or traps for hydrocarbons. The resolution provided by the seismic data is such that the general structural and stratigraphic properties of the formations can be delineated. The detailed variations, which are of interest for reservoir characterization, occur at sub-reservoir scales (less than 10 m) and are difficult to image using the surface seismic data. For near surface investigations, the objective is to image variations which have a scale on the order of meters. The sources suitable for deep exploration are inadequate for the investigation of the near surface, due to the long wavelength seismic waves generated. New ideas for sources are required in order to measure the seismic properties of the near surface. The use of piezoceramic bender elements for field investigations is a new idea which appears to have significant potential.

For many years bender elements have been utilized by scientists and geotechnical engineers in the laboratory to measure the low strain shear modulus of cohesionless sediments (Shirley and Hampton, 1978; Dyvik and Madshus, 1985; Yan, 1990). In most applications the bender elements are inserted at either end of a testing apparatus and the travel time of a shear wave is measured using an oscilloscope. This type of measurement is directly analogous to the laboratory measurement of elastic wave velocities using ultrasonic, piezoelectric crystals (Hughes and Cross, 1951; Goertz, 1994). The primary benefit of the

bender elements is the enhanced coupling with the cohesionless medium, that enables the propagation of elastic waves in the 5 to 25 kHz range. Bender elements have been used extensively in the laboratory and have proven to be a good source and receiver of elastic waves. In particular, they have been very effective as a source and receiver of shear waves. A logical extension of the laboratory research is the field use of the bender elements for shallow seismic investigations.

The focus of this thesis is to outline the development of bender elements and their use for a number of geophysical applications. In Chapter 2, the bender element response in a bucket of sand is examined at a fixed separation and in a sandbox at varying separations. The bucket of homogeneous, dry sand enabled the bender waveform to be analyzed under carefully controlled laboratory conditions. The sandbox, which has a mixture of grain sizes and types and was partially saturated, is more representative of a true soil. The sandbox was used to study the variation of the shear waveform with bender separation in a non-homogeneous material. The sand bucket and sandbox experiments are analogous to using the bender elements as a probe to measure in situ velocity and show the potential for near surface field studies. Chapter 3 examines the insertion of the bender elements in a Plexiglas cell. The cell was packed with sand and saturated with both water and silicon oil to measure changes of shear wave velocity as a function of confining pressure. The bender elements have demonstrated significant versatility in the laboratory measurement of elastic wave velocities.

The integration of raw piezoceramic bender elements into bender element assemblies is a fundamental part of the thesis. The assemblies were constructed as rugged devices capable of withstanding pressures of at least 200 kPa and immersion in a variety of fluids. A Swagelok feedthrough is a key component that enables the mounting of the assembly in a number of different laboratory apparatuses. These include, but are not restricted to, a confining pressure cell used to measure changes in elastic wave velocity due to fluid saturation, and a steam flood apparatus which has the potential to measure changes of elastic wave velocity during a laboratory steam flood.

The development of additional tools to examine the near surface will enhance our ability to image the near surface remotely. This has significant impact in the investigation of contaminated sites where disturbances must be minimized. Before the benders can be used for near surface studies, they must be fully evaluated in the laboratory to establish the key variables which impact the response. The refinement of the bender element response in the laboratory will lead directly to future applications in the field.

Chapter 2

BENDER ELEMENTS

2.1 Introduction

The development and use of geophysical instrumentation has provided excellent insight into the structure of the subsurface. Seismic techniques involve the generation of seismic waves with some type of source and the monitoring of the transmitted, reflected and refracted seismic energy with some type of receiver. Different types of sources and receivers have been utilized by the exploration industry for many years. The focus has been on deep investigations. For shallow work the challenge is to develop new sources and receivers that are better suited to a shallow, typically cohesionless, environment.

The key to obtaining high resolution in a shallow seismic experiment lies both in the frequency content of the source and the frequency response of the receiver. The shallow subsurface consists of a series of closely spaced layers of cohesionless material, that require a short seismic wavelength to clearly resolve. The resolution of seismic reflection data determines the minimum layer thickness that can be imaged and is typically taken to be one quarter of a wavelength. For a seismic wavelength of 10 cm and a velocity of 200 m/s a center frequency of at least 2 kHz is required. In order to transmit a seismic pulse the source must properly couple with the medium. The coupling of the source is determined by the nature of the physical contact with the medium, that will vary with frequency. So the development of a source for shallow investigations in cohesionless material requires good coupling in the kHz frequency range. The bender elements utilized in this thesis meet these requirements.

The focus of this chapter is to examine the use of bender elements for a number of applications. The nature of the propagating pulse is examined for both shear and compressional waves in a bucket of sand. The short compact nature of the waveform

demonstrates that bender elements can be used for both first arrival velocity measurements and possibly for attenuation and reflection imaging applications. The elements were also evaluated in a sandbox to determine the effect of bender separation on the received waveform. The bender waveform was clearly visible out to a distance of 35 cm. The testing of the bender elements has revealed the remarkable versatility of the elements as a laboratory tool for measuring elastic wave velocities. Further evaluation is required in order to use the elements as a component of geophysical instrumentation for shallow seismic applications.

2.2 Bender Element Description

Bender element technology has been used for the last 16 years to measure shear wave velocities in cohesionless sediments. Shirley and Hampton (1978) used bender elements to measure the shear wave velocity in clay slurries and were able to measure velocities as low as 2 m/s. The primary reason that bender elements were evaluated in this thesis is due to their proven effectiveness as a source and receiver of shear waves in the various apparatus commonly used by geotechnical engineers. De Alba et al. (1984) mounted bender elements in the end plates of a triaxial cell. Dyvik and Madshus (1985) also placed bender elements in a triaxial cell and used them in simple shear and oedometer devices as well. These devices are used by geotechnical engineers to make measurements of the large strain shear strength and consolidation of cohesionless sediments. In addition to the large strain shear characteristics the small strain or elastic shear modulus is also desired.

In the past, the elastic shear modulus was established by using the resonant column test on a separate cohesionless specimen. The use of bender elements enabled geotechnical engineers to make measurements of the elastic shear modulus (referred to as G_{\max}) within the same apparatus. The emplacement of bender elements within a resonant column by Dyvik and Madshus (1985) clearly demonstrated that the shear moduli obtained using the two techniques were identical. Bender elements were used by Yan (1990) and Gohl (1990) in the Civil Engineering Department at the University of British Columbia. These studies provided

the design procedures and made available the raw bender elements which were used in this thesis.

The benders are better than piezoelectric crystals for transmitting and receiving shear impulses due to their lower resonant frequency, which better matches the natural resonance of a cohesionless sand pack (Shirley and Hampton, 1978). The strains generated by the bender elements within the sand pack are approximately 10^{-7} (Thomann and Hryciw, 1990) which ensures that plastic deformation of the sand pack surrounding the elements will be minimized. A diagram of a bender element is shown in Figure 2.1. The bender consists of a sandwich of piezoceramic materials, with nickel plates on the outside, that is attached rigidly to a bearing plate. The ceramic is polarized in a particular direction and when a voltage is applied to the nickel plates, one of the layers expands and the other contracts. The result is a flexure of the element, that when coupled to a sand pack serves as a source of elastic waves. In a similar fashion the flexure of the receiver element by the passing wave generates a voltage in the attached leads that can be amplified and displayed.

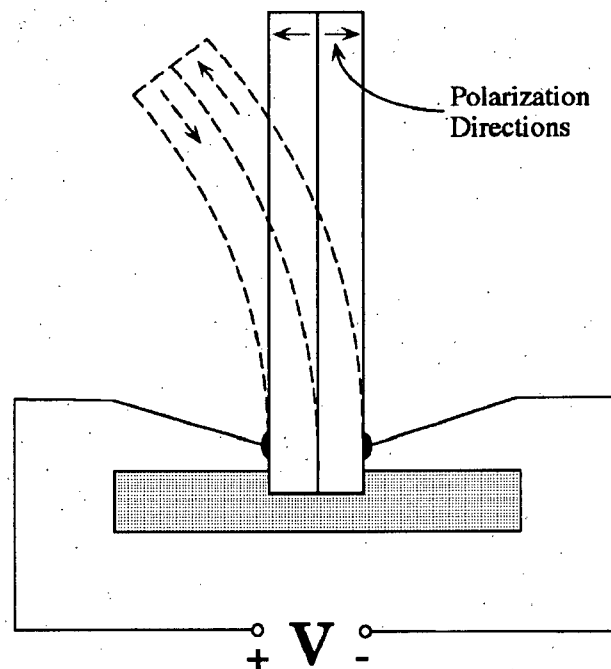


Fig. 2.1. A diagram of a piezoceramic bender element. The dashed lines show the flexure which results when a voltage is applied to the nickel plates on the outside of the element.

2.3 Experimental Procedures

The primary objective of this chapter is to evaluate the bender elements as a source for and receiver of elastic waves. The experimental techniques are simple and the experimental data are repeatable. The design of the bender element assemblies is detailed below, as well as the measurement techniques used in the bucket of sand and in the sandbox.

2.3.1 Bender Building

The construction of the bender elements is critical to the final performance of the elements both in the confining pressure cell and in the sandbox. The benders were built in a series of steps with the primary design criteria being the optimization of the free-air resonance, and the repeatability of the design for two benders. The benders started out as raw piezoceramic plates, which were then mounted and coated to form the bender element assemblies.

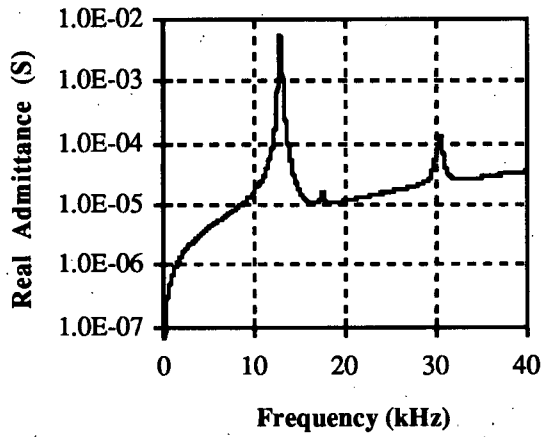
A key component of the design process was the use of an impedance analyzer to monitor the electrical and mechanical characteristics of the bender elements. The equipment used to measure admittance was a HP 4192A low frequency impedance analyzer. The analyzer is capable of measuring either impedance or admittance, both real and imaginary components, from 5 Hz up to 13 MHz. The admittance option was chosen for the bender elements due to the high DC resistance of the elements. The analyzer was interfaced with a Macintosh computer and a program was run that makes the impedance analyzer automatically sweep through a series of frequencies, testing the admittance at each step and sending the data to a file on the Macintosh.

The bender elements start out as 0.5 in (1.3 cm) square piezoceramic plates available from Piezo Electric Products Inc. as product number S500N (with nickel plates). The nickel plates facilitate the soldering of wires to the elements. The first step in the construction involved the removal of oxidation from a small dot at the center of one of the square sides, close to the edge. A solder connection was made on the other nickel plate, directly opposite

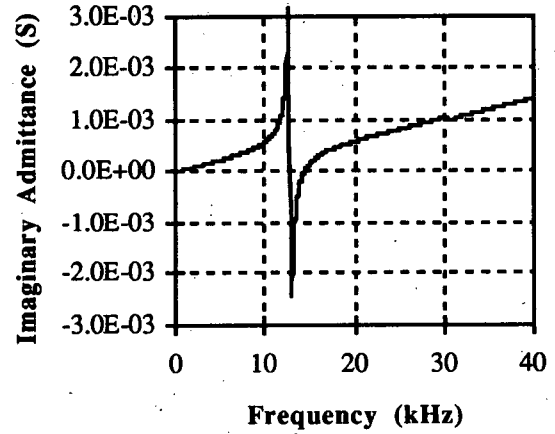
the solder point, so another dot was cleared of oxidation. The objective was to make the solder connections as small as possible, because the solder acts to stiffen the bender element, reducing the flexure in response to an applied voltage. The benders are high impedance and the currents sent to the elements or generated by them are extremely small, so very small wires (AWG 30) were used. The smaller wires also have a smaller capacitance, which is another favorable characteristic for noise reduction. The wires were soldered to the element with the free ends directed to one of the corners.

The raw benders with two wires connected were then attached to the impedance analyzer. A plot of the frequency response for each element is shown in Figures 2.2 and 2.3. The elements were designated green and blue, which corresponds to a color code on one of the lead wires that was used to differentiate the elements and to tag a common side for polarity tracking. The frequency response is reasonably simple with a resonant peak at 12.8 kHz and 30.4 kHz for the blue bender and at 11.4 kHz and 26.9 kHz for the green bender. The differences between the benders is attributed to the slightly different thicknesses. The resonant frequency of the elements, specified by the manufacturer, for a cantilever mounting is 1520 Hz, which is distinctly different from the resonant frequency of the green and blue elements.

The next stage in the building was the mounting of a bearing plate to act as a cantilever base. A 1 mm by 5 mm by 12.5 mm Plexiglas rectangle was used with a 0.5 mm wide groove cut to accommodate the bender. The bender was glued into the groove using a quick bonding cement (Loctite Super Bonder 495). The admittances of the benders with the bases attached are shown in Figures 2.4 and 2.5. The addition of the base has added a series of additional resonant peaks. It was noticed during the gluing process that the benders seemed to be of slightly different thicknesses. This resulted in both a loose and a tight fit into the groove. This difference seemed to be the cause of differences in the admittance curves, that were also obvious before the benders were glued to the base (see above). The differences in admittance were not considered significant. The choice of material for the cantilever base

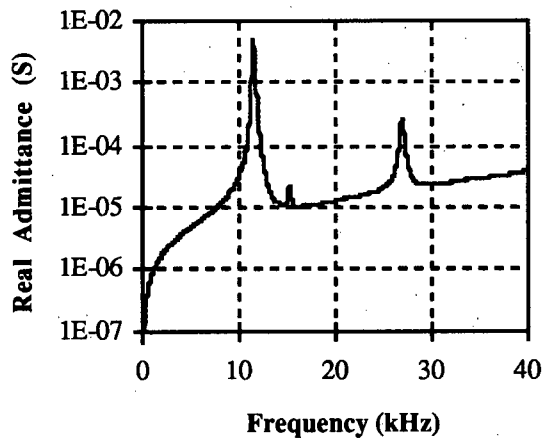


(a)

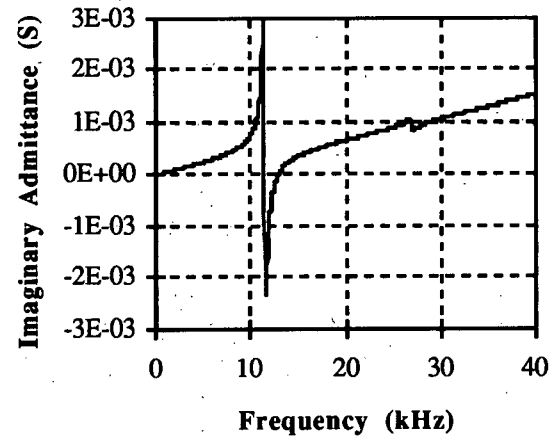


(b)

Fig. 2.2. Graphs of the admittance as a function of frequency for the blue bender with leads attached. (a) Real Admittance (b) Imaginary Admittance.

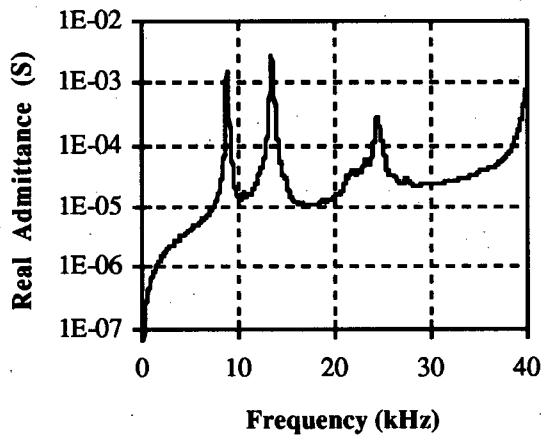


(a)

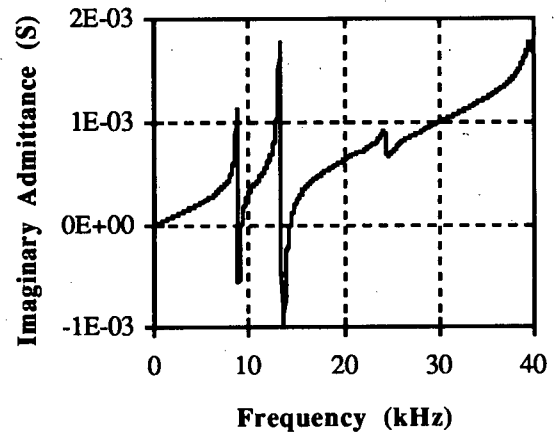


(b)

Fig. 2.3. Graphs of the admittance as a function of frequency for the green bender with leads attached. (a) Real Admittance (b) Imaginary Admittance.

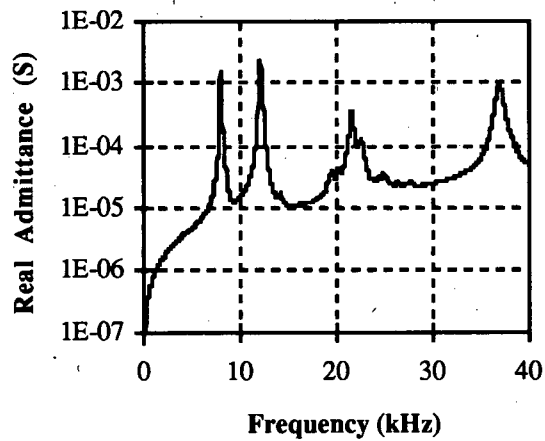


(a)

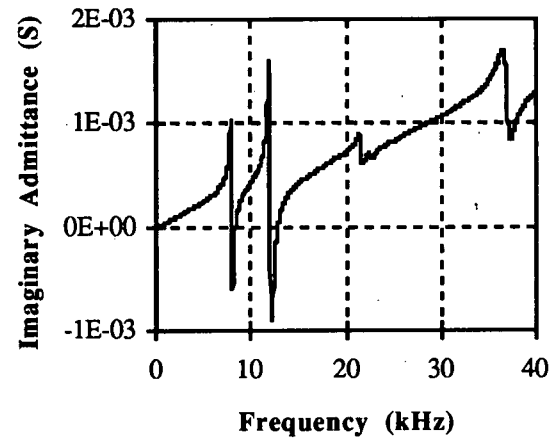


(b)

Fig. 2.4. Graphs of the admittance as a function of frequency for the blue bender with Plexiglas base attached. (a) Real Admittance (b) Imaginary Admittance.



(a)



(b)

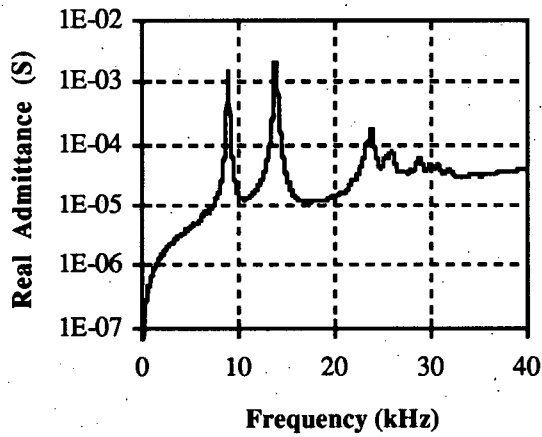
Fig. 2.5. Graphs of the admittance as a function of frequency for the green bender with Plexiglas base attached. (a) Real Admittance (b) Imaginary Admittance.

is critical to the final response of the element. It must be non-conductive to avoid shorting the plates. Stiffer materials will result in lower resonant frequencies than softer materials.

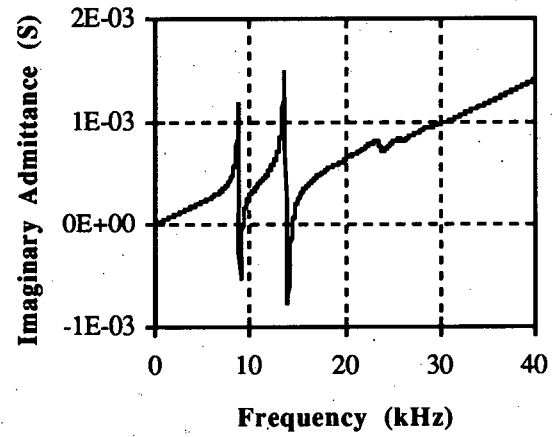
The next step involved coating the benders with a very thin, uniform coating of epoxy. The benders were operating in contact with water, so an electrical insulating layer was needed around the elements. Sun Cure epoxy, which is a slow curing, low shrinkage epoxy was used. In order to obtain thin coatings, the epoxy was allowed to partially harden, before application. The sheeting action of the very fluid epoxy caused most of it to drip off the elements, leaving a very thin coating. The admittance of the elements after one coat of epoxy is shown in Figures 2.6 and 2.7. The resonant peaks have been slightly damped by the thin coating of epoxy.

The bender elements were fabricated into assemblies which were designed to attach to the inside of a Plexiglas cell. In order to isolate the lead wires from the possibly conductive contents of the cell, and to provide a means of feeding the wires through the sides of the cell, the wires were encased in a straightened section of Swagelok plastic, 1/8 inch tubing. The tubing was inserted into a Swagelok bulkhead feedthrough, which provides a vacuum proof, adjustable attachment to the side of any container where measurements of elastic wave velocities are desired. After the lead wires had been encased, the benders were coated once again with Sun Cure epoxy, which also served to seal the short section of exposed wires. The admittance of the elements at this stage is shown in Figures 2.8 and 2.9. Some additional resonant peaks are obvious, but the general character remains the same.

The bender assemblies were then coated with two additional thin coatings of epoxy. The final admittance of the elements is shown in Figures 2.10 and 2.11. With each step, the resonant peaks have been reduced in amplitude, demonstrating the damping effects of the epoxy on the bender motion. The free air admittance curves for each bender are very similar which demonstrates the electrical and mechanical similarity of the two elements. The free air resonances are not really indicative of the performance of the benders in contact with a sand pack. Figures 2.12 and 2.13 show the admittance curves of the benders in contact with a dry

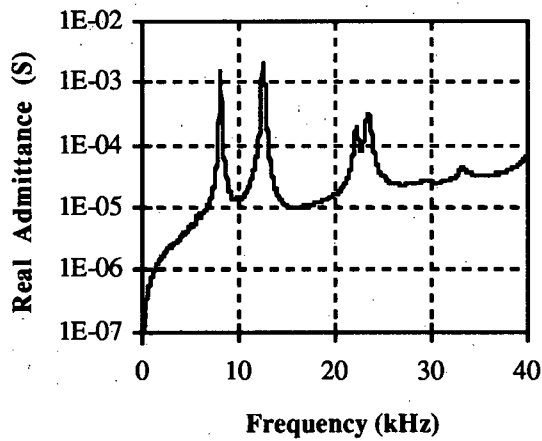


(a)

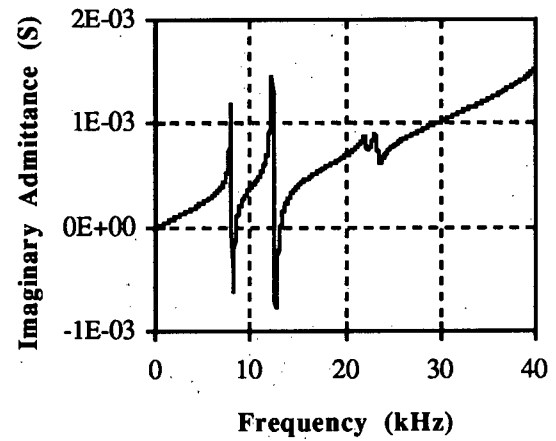


(b)

Fig. 2.6. Graphs of the admittance as a function of frequency for the blue bender with one coat of Sun Cure epoxy. (a) Real Admittance (b) Imaginary Admittance.

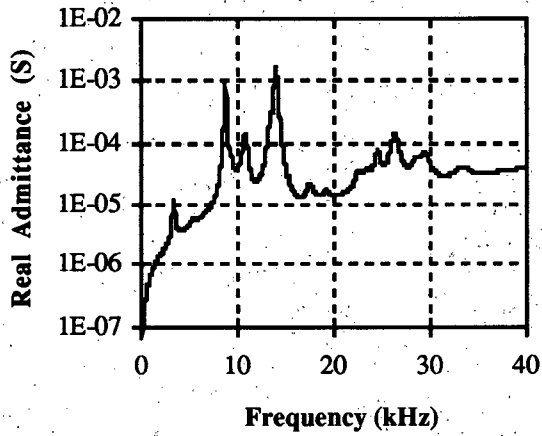


(a)

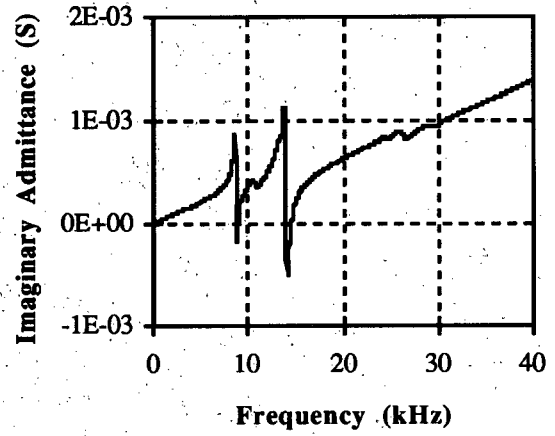


(b)

Fig. 2.7. Graphs of the admittance as a function of frequency for the green bender with one coat of Sun Cure epoxy. (a) Real Admittance (b) Imaginary Admittance.

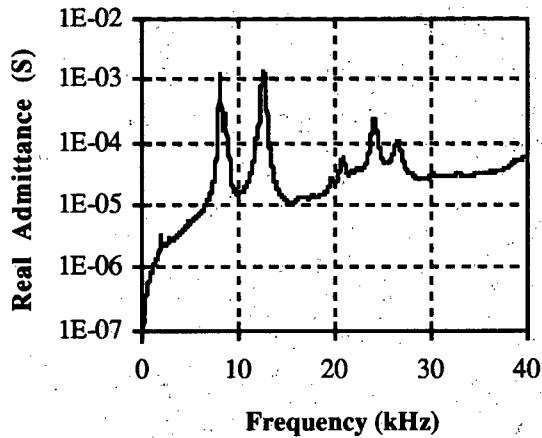


(a)

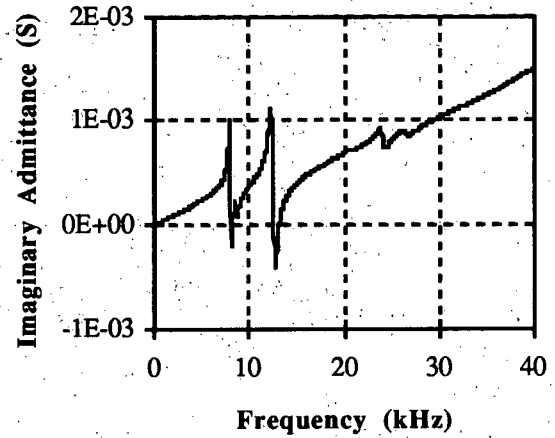


(b)

Fig. 2.8. Graphs of the admittance as a function of frequency for the blue bender with Swagelok tubing attached and another coat of epoxy. (a) Real Admittance (b) Imaginary Admittance.



(a)



(b)

Fig. 2.9. Graphs of the admittance as a function of frequency for the green bender with Swagelok tubing attached and another coating of epoxy. (a) Real Admittance (b) Imaginary Admittance.

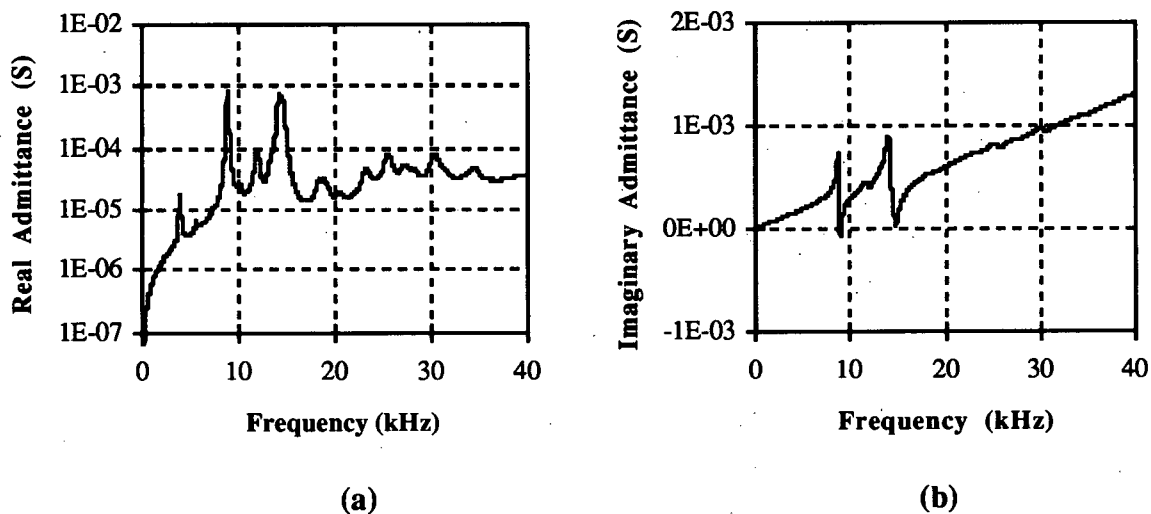


Fig. 2.10. Graphs of the admittance as a function of frequency for the blue bender after final coating of epoxy. (a) Real Admittance (b) Imaginary Admittance.

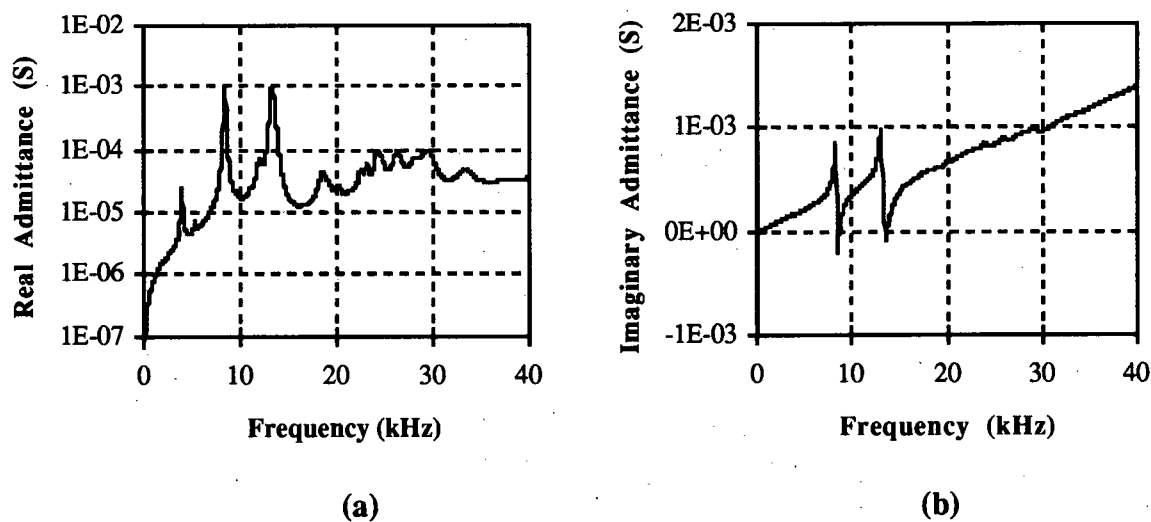
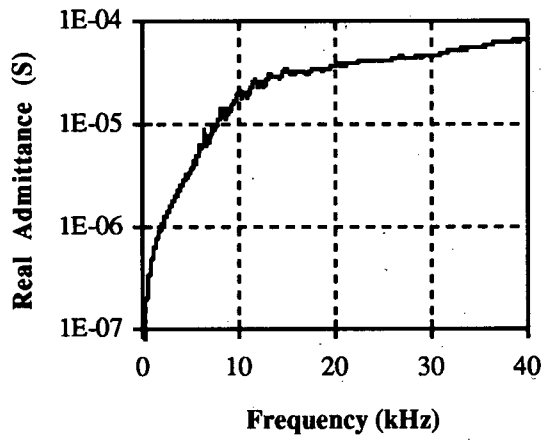
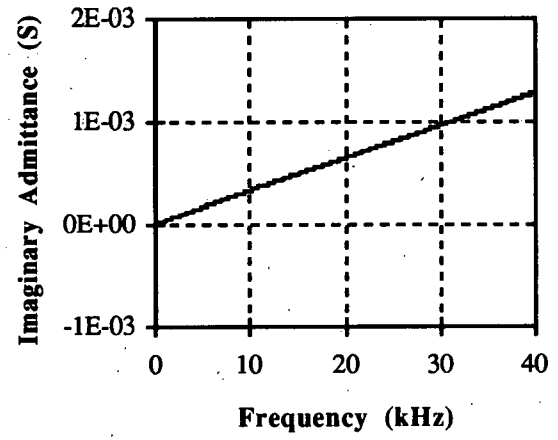


Fig. 2.11. Graphs of the admittance as a function of frequency for the green bender after final coating of epoxy. (a) Real Admittance (b) Imaginary Admittance.

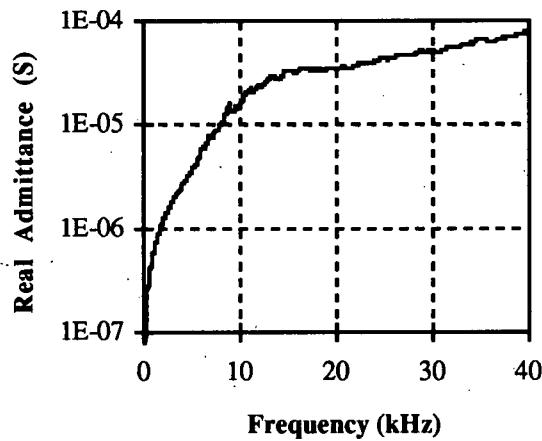


(a)

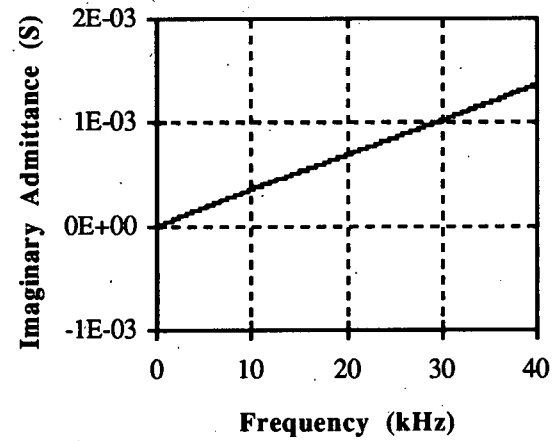


(b)

Fig. 2.12. Graphs of the admittance as a function of frequency for the blue bender in contact with a sand pack. (a) Real Admittance (b) Imaginary Admittance.



(a)



(b)

Fig. 2.13. Graphs of the admittance as a function of frequency for the green bender in contact with a sand pack. (a) Real Admittance (b) Imaginary Admittance.

sand pack. All resonant peaks have been damped out, demonstrating the dominance of the sand pack confinement on the bender response. The similarity of the blue and green bender elements becomes apparent when the admittance curves are compared to those from an earlier bender design.

A different bender design was used for the first prototype of the saturating cell. This design was comparable to that used by Yan (1990) in a hydraulic gradient apparatus. The design involves the soldering of the benders to a piece of etched circuit board. Long lead wires consisting of AWG 18 stranded copper wire were then soldered to the circuit board. A series of acrylic and nitrile rubber coatings were then applied to insulate the benders from the sand pack. The benders were designated #1 and #2. The admittance curves for the two benders constructed using this alternative technique are shown in Figures 2.14 and 2.15. The free air resonant peaks are significantly different. This is attributed to the non-uniformity of the soldering technique used to affix the benders to the bearing plate.

The design of the bender elements for the new confining pressure cell, using the impedance analyzer as a quality control and comparative device has resulted in the building of two very similar, rugged, elements for the measurement of elastic wave velocities under a variety of conditions. The data contained within the thesis illustrates the successful application of the elements.

2.3.2 Sand Bucket Experiments

The sand bucket was used to get an idea of the general waveform characteristics in a dry, homogeneous sand pack. The bucket makes it easy to perform the experiments in the lab, where the instrumentation can be easily controlled. The waveform shape is examined for both shear and compressional waves and the linearity of the response to the input voltage is evaluated for shear waves.

The benders were inserted in the bucket of loose, cohesionless sand with a reasonable amount of sand (~10 cm) placed on top. The objective was to surround the benders with a

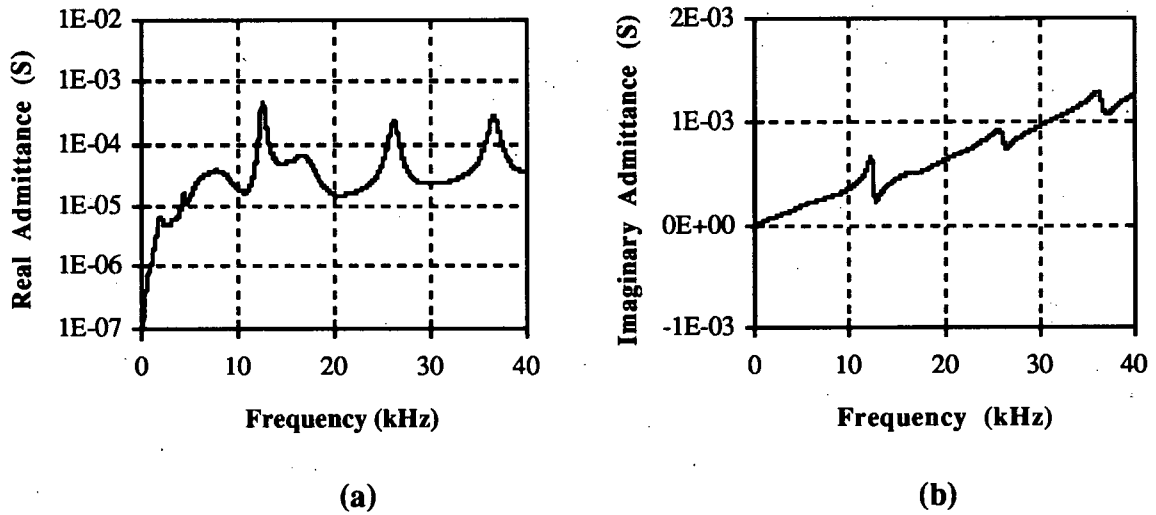


Fig. 2.14. Graphs of the admittance as a function of frequency for bender #1, attached to a circuit board and coated with acrylic and nitrile rubber. (a) Real Admittance (b) Imaginary Admittance.

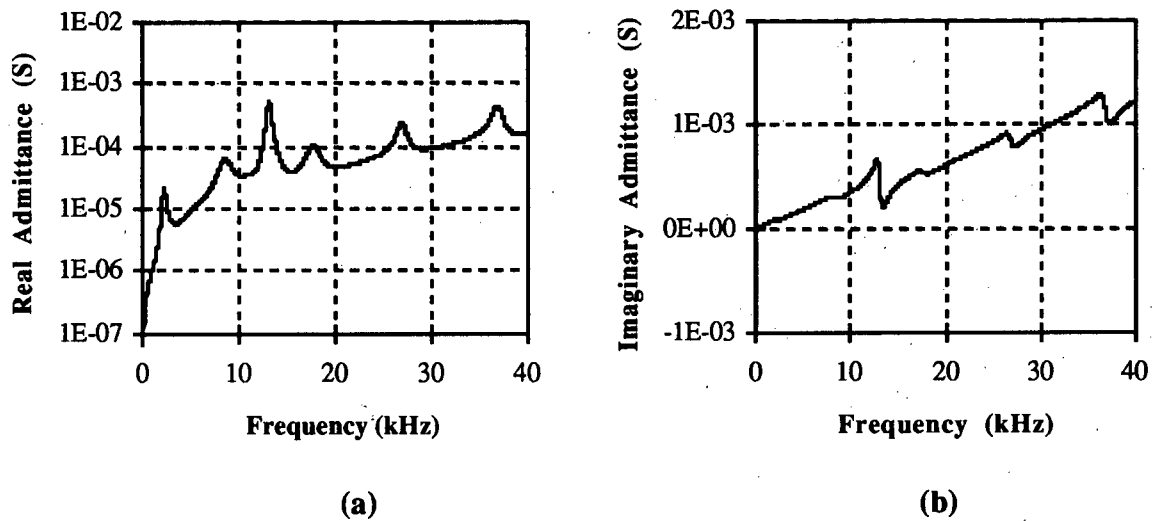


Fig. 2.15. Graphs of the admittance as a function of frequency of bender #2, attached to a circuit board and coated with acrylic and nitrile rubber. (a) Real Admittance (b) Imaginary Admittance.

homogeneous sand pack, with potential reflecting surfaces far from the elements. The alignment of the elements and approximate separation were noted. It is difficult to obtain a good alignment, because the benders are connected to bulky wires, and there is no fixed mounting. The approximate orientations were close to the orientations required to separately send and receive shear and compressional waves, with minimal interference. The orientation of the elements determines whether the first arriving waveform will represent compressional or shear waves.

To examine shear waves, as the first arriving seismic energy, the source and receiver elements are placed in the same plane with the edges of the elements aligned with each other, and the tips away from the bearing plate, pointed towards each other. The average velocity of the sand pack between the elements is computed by using the separation of the bender tips (Dyvik and Madshus, 1985). The benders can be re-oriented to act as a source of compressional waves. When the benders are placed parallel to each other, but perpendicular to a line between them, the bender flexure will create a particle motion associated with compressional waves.

The minimum separation of the elements is governed by the wavelength of the elastic waves generated. In order to minimize the effect of the near field signal Yan (1990) recommended a minimum separation of two wavelengths. Shirley (1978), who did the pioneering research with bender elements in cohesionless sediments, demonstrated that the greatest sensitivity of the elements will be at a frequency where the wavelength of the elastic wave is twice the length of the elements. For the elements used in this thesis, two wavelengths will be approximately 5 cm, which was the minimum separation used.

The source bender element is connected to an IEC F33 function generator, which is capable of putting out a 20 V peak-to-peak square wave with a rise time of 60 nsec. The receiver bender has its individual leads attached through the shielded center conductor of coax cables to the differential inputs of a Stanford Research Systems SR560 voltage preamplifier. The use of the differential inputs allows the subtraction of any coupled noise

developed in the cables, typically produced by overhead fluorescent lighting and nearby transformers. The amplifier also allows the bandpass filtering of the signal. Typically a 300 Hz to 1 MHz bandpass was used with 6 dB/octave slopes on the high and low ends. The output of the amplifier is sent to a Tektronix TDS 420 digital oscilloscope, where the signal can be averaged to further reduce any noise. The oscilloscope is triggered by the function generator to establish the zero time for the traces. The oscilloscope is also capable of storing up to four signals in memory. This allows for the transfer of the data to a Macintosh Quadra computer using the Labview software package.

The driving waveform is critical in determining pulse shape. The purpose of the driving waveform is to flex the bender element in a characteristic manner. For first arrival measurements it is important to have as much flexure as possible occurring early. The early flexure will be associated with the first lobe of the waveform arriving at the receiver element. The larger the first lobe, the easier it is to pick the first arrival, especially in the presence of noise. For the sand bucket experiments a 3 V peak-to-peak square wave was used with a rise time of 60 nsec and a frequency of 5 Hz. For the bender linearity experiment a series of square wave voltages was used: 0.3, 1.0, 3.0 and 10 V.

2.3.3 Sandbox Experiments

The sand bucket experiments gave a good indication of the bender waveform characteristics, but the separation of the source and receiver elements was limited by the physical size of the bucket. The insertion of the benders in a sandbox enabled the evaluation of the benders at larger separations. The sandbox was filled with poorly sorted sand with grain sizes ranging from silt to centimeter scale pebbles. The sand is fully saturated with water at a depth of 21.6 cm and partly saturated at the surface. The sandbox was constructed in the Geophysics Department at the University of British Columbia for undergraduate IP (induced polarization) experiments. The dimensions of the sandbox are: 1.19 m by 1.78 m. The sandbox enables bender experiments to be carried out without reflections and refractions

from the sides.

A diagram of the sandbox experiment is shown in Figure 2.16. The pulse generator sends a square wave to the source bender element (designated S) and also triggers the oscilloscope to obtain the "zero" time. The elastic wave travels through the sand and is picked up by the receiver bender element (designated R). The voltage change induced by the flexure of the receiver element is amplified and then displayed on the oscilloscope. The oscilloscope averages a series of received waveforms to improve the signal to noise ratio. The frequency of the square wave is chosen so that there is no interference from the previous excitation of the elements. The experiments were all carried out using a 5 Hz, 3 V square wave.

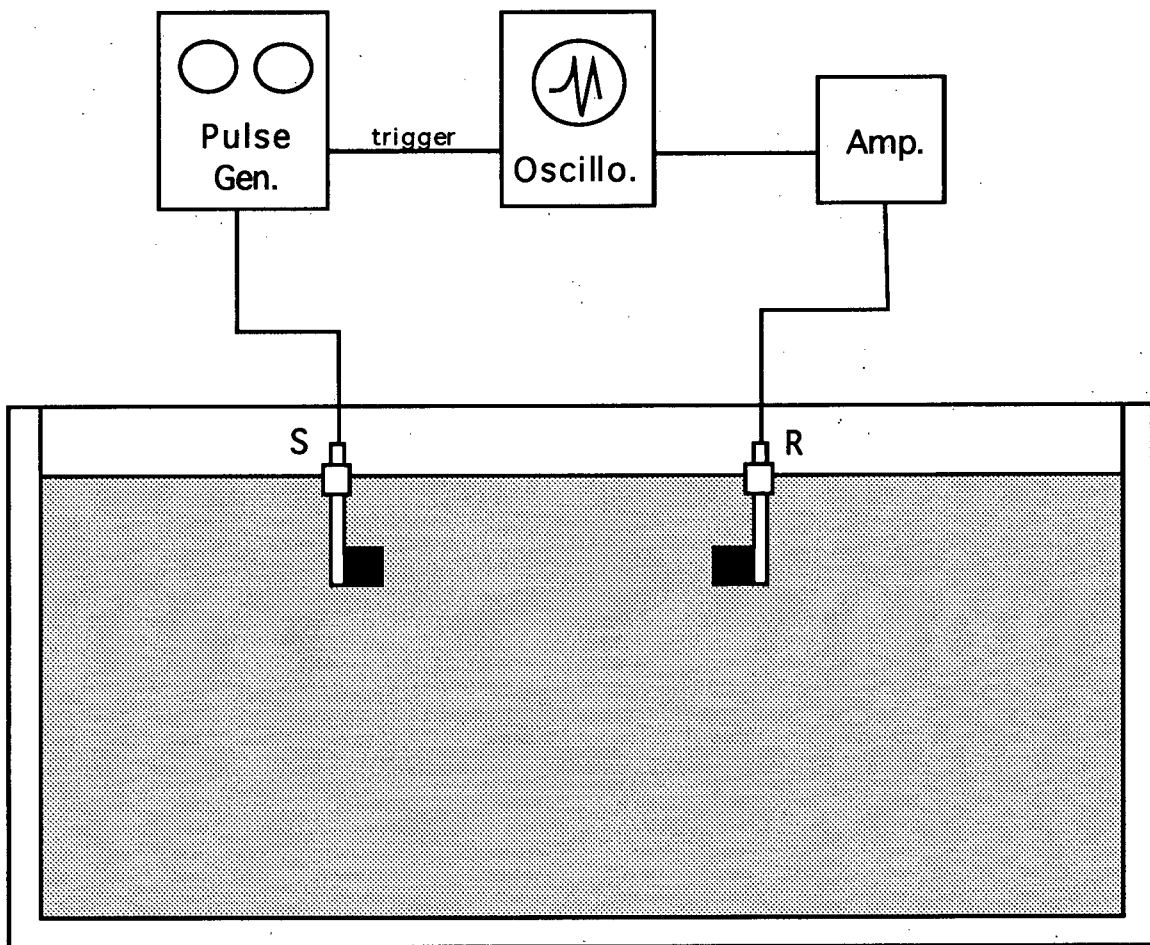


Fig. 2.16. Diagram of the sandbox experiment.

The benders were inserted into the sand at a depth of 4 cm in a vertical orientation with the tips pointing towards each other, at approximately the same elevation. This orientation is optimal for generating and receiving shear waves. To enhance the coupling the sand was then packed by hand. The source element remained in place while the receiver element was moved, to reduce variations due to the sand packing around the elements. The initial separation of 7.6 cm is close to the separation used in the sand bucket, so a known reference waveform could be identified. The separation was then increased in approximately 10 cm increments until the first arriving waveform became difficult to identify on the oscilloscope. The maximum separation utilized was 35.6 cm. The benders were inserted into the sand at the approximate locations then the separation of the elements was determined by measuring the distance between the plastic posts protruding from the sand surface and subtracting 2.5 cm, which represents the offset of the bender tips from the posts.

2.4 Discussion and Results

The bender elements proved to be a highly effective source and receiver for both compressional and shear waves in a cohesionless sand. The source bender generates a narrow pulse of known polarity and simple character, while the receiver bender readily converts the arriving seismic energy into a measurable electrical signal. Both the sand bucket and the sandbox experiments were effective in the evaluation of the bender waveform.

The nature of the waveform is critical to the evaluation of the bender elements for both laboratory and field usage. For travel time/velocity measurements, the amplitude of the first lobe determines how easily the first arrival can be picked on an oscilloscope. In addition, the use of the bender elements for any type of reflection profiling requires that the waveform be reasonably compact in time, in order to separate closely spaced reflections. The bender elements were first evaluated in a bucket of sand to get an idea of the "raw" bender waveform for both compressional and shear waves. This simple experiment clearly identifies the compact nature of the bender waveform.

2.4.1 Benders as a Source of Shear Waves

The development of a shear wave source and receiver is particularly important. In cohesionless material, the small changes in shear wave velocity associated with fluid saturation are often solely due to a change in density. This is in direct contrast to compressional waves where very large changes in velocity are associated with fluid saturation. This reduced response to fluids makes shear waves a good discriminator of lithologic units and lithologic boundaries. The benders seem to be ideal for the generation of shear waves. This is due to their plate-like geometry which encourages the generation of a wave with particle motion given by the plate flexure direction and wave motion perpendicular to particle motion. This property has been recognized and utilized extensively by geotechnical engineers (Dyvik and Olsen, 1989; Thomann and Hryciw, 1990; and Yan, 1990).

An example of a shear wave waveform, measured with a source-receiver separation of 5 cm, is shown in Figure 2.17a. The Fourier spectrum of the waveform is shown in Figure 2.17b. The waveform is compact in time confirming the broadband nature of the amplitude spectrum. The first arriving lobe is large and the standout from the background noise is extremely good, making the measurement of first arrival times feasible. Prior to the arrival of the S-wave (indicated in Figure 2.17a) another low amplitude arrival is interpreted as a near field arrival. This near field arrival is expected from elastic wave theory and has been correlated with the waveform of bender elements in a shear orientation by Yan (1990). The arrival time of the shear wave is approximately 750 μ sec. With a separation of approximately 5 cm, the loose, dry sand has a shear wave velocity of 70 m/s.

The voltage of the input square wave was varied to examine the effect on the received waveform. The variation of shear waveform with input voltage is shown in Figure 2.18. The amplitude spectra demonstrate that the higher input voltages result in a lower dominant frequency. The first arrival pick is labeled in Figure 2.18 and was taken as the time at which

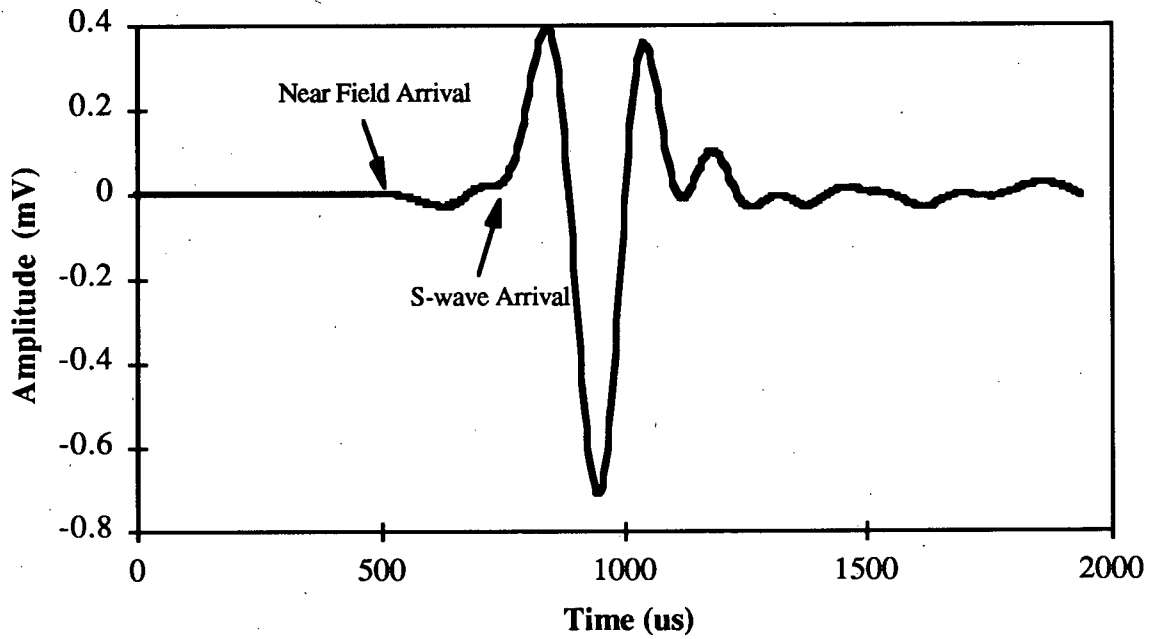


Fig. 2.17a. A waveform from the sand bucket experiment with the benders in an orientation favorable for shear waves.

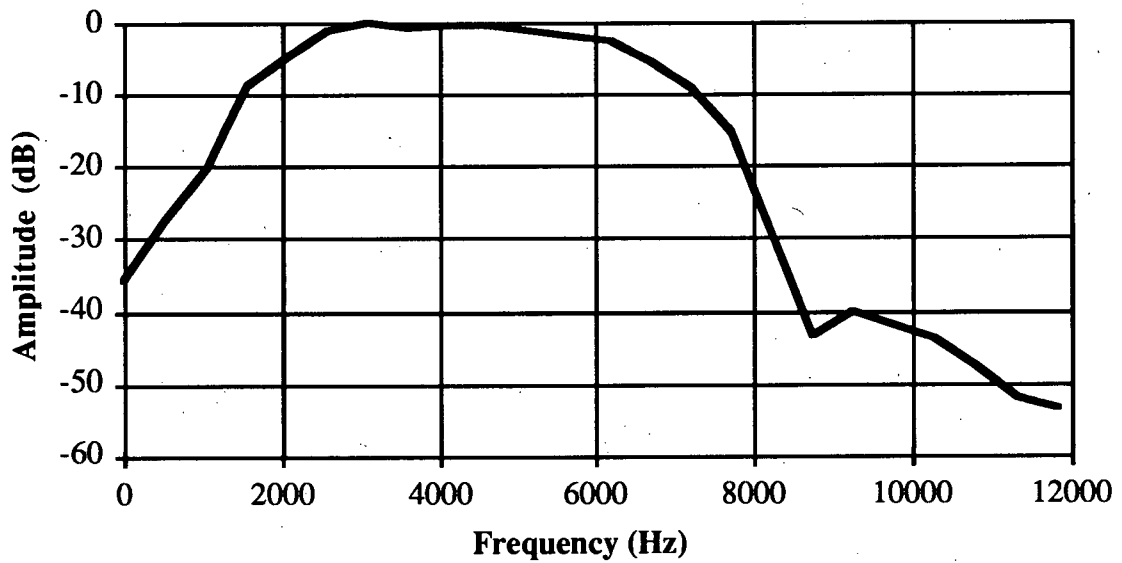


Fig. 2.17b. The amplitude spectrum of the waveform in Figure 2.17a.

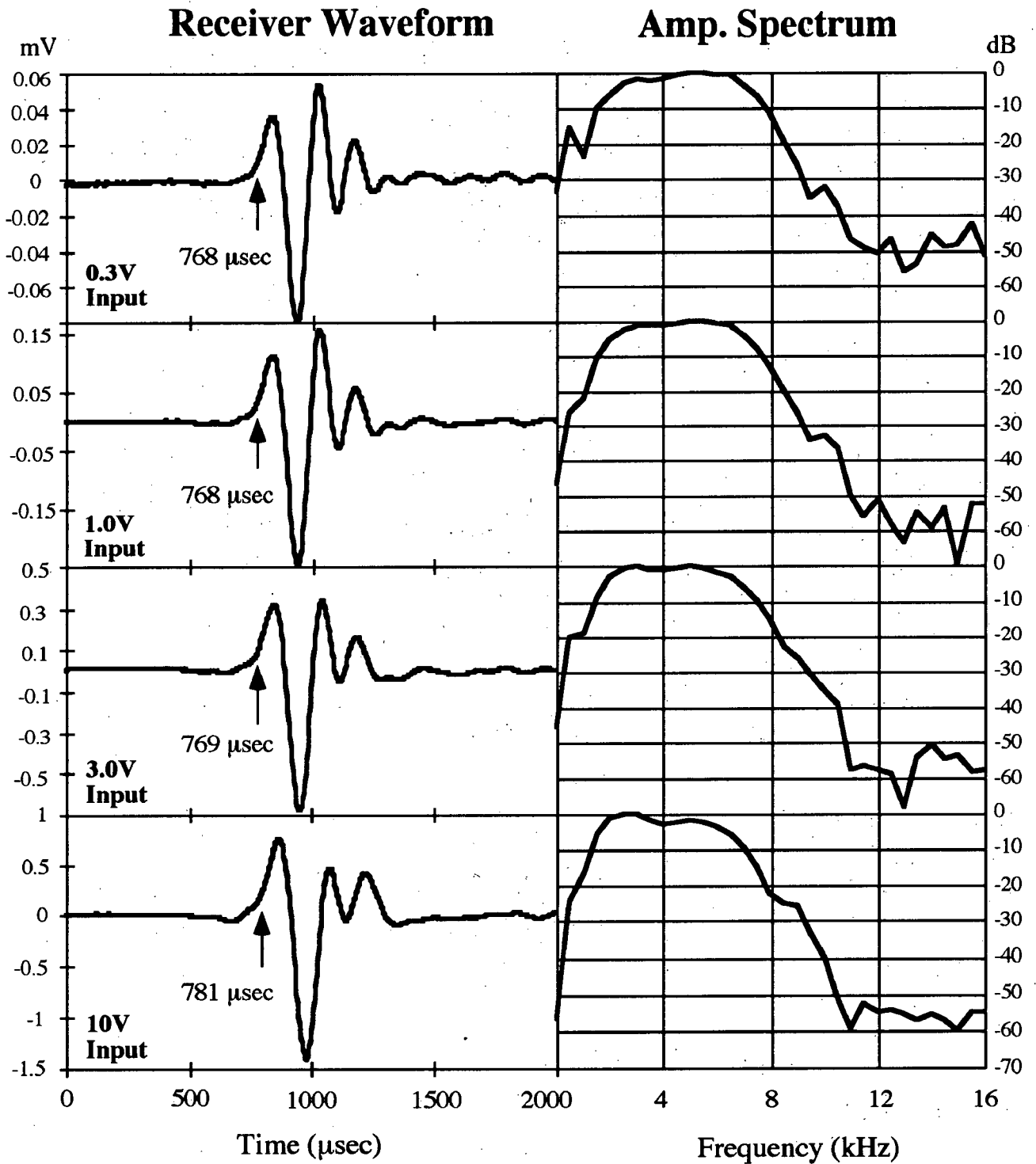


Fig. 2.18. Diagram illustrating the variation in shear wave waveform with input voltage. The arrows and numbers indicate the time at which the waveform is at 20% of the first peak amplitude.

20% of the amplitude of the first peak is achieved. This ensures the pick is not affected by the variation in signal to noise or the variations in the near field arrival. The pick shows little variation up to 3 V and varies by only 1.5% with an input of 10 V. The final lobes of the waveform appear to be affected the most by the variation in input voltage. In order to quantify variations of the waveform with input voltage, the amplitude of the initial peak and trough were picked. The data is shown in Figure 2.19 and Figure 2.20 as graphs of output voltage versus input square wave voltage. A parabola was fitted to the four data points on each graph to give an unbiased indication of the data trend. The graphs demonstrate the linear nature of the output with respect to the input up to 3 V. The variation at 10 V is attributed to the plastic deformation of the sand pack, due to the higher amplitude bender motion. The variations in the input square wave with voltage will also contribute to variations in the received waveform.

From the simple experiment in a bucket, the bender elements have proven to be a good source for and receiver of shear waves. The waveform is small and compact with a frequency content determined by the natural resonances of the coupled sand pack. The orientation of the benders determines the type of waves likely to be seen first by the receiver bender element. By re-orienting the benders they can also be used to generate and receive compressional waves.

2.4.2 Benders as a Source of Compressional Waves

Compressional waves are generally easier to generate than shear waves. The impulsive nature of explosive and impact sources are excellent generators of compressional waves. The use of the benders for compressional waves is considered to be important because the measurement of both shear and compressional waves with the same source and receiver makes the elements more versatile, and the availability of both shear and compressional wave velocities in a similar frequency range fully identifies the elastic properties of a material.

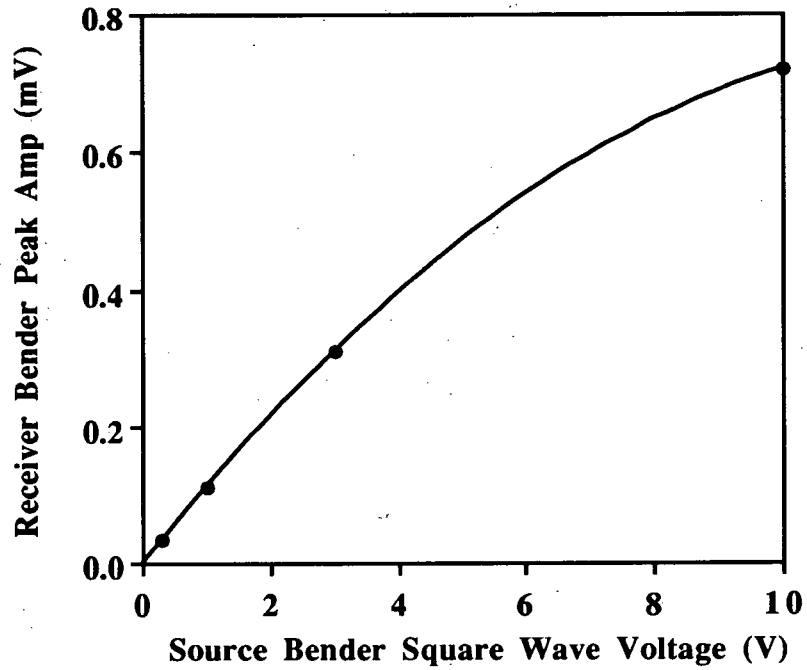


Fig. 2.19. Graph of the receiver bender output amplitude as a function of source bender input square wave voltage. Picks were made of the first peak following the shear wave arrival. The line represents the least squares fitting of a parabola to the four data points.

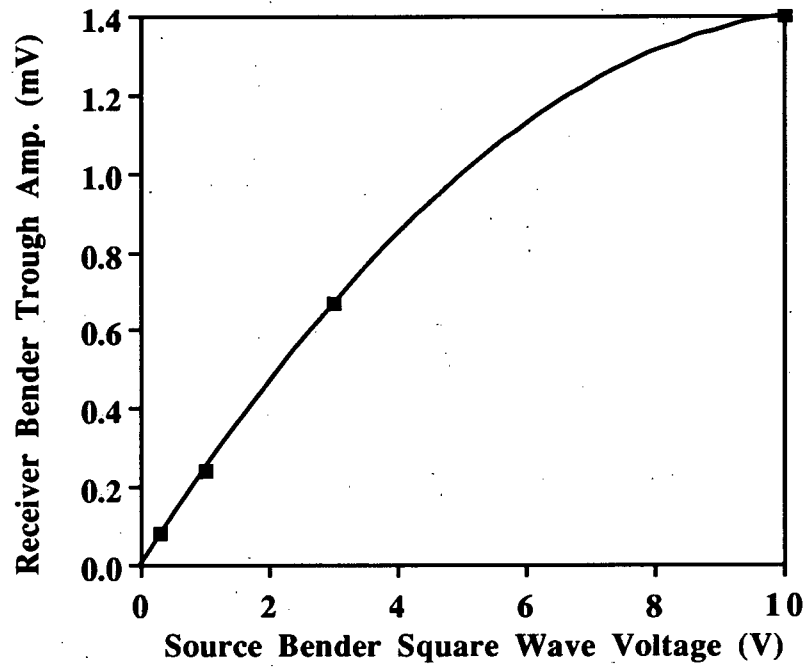


Fig. 2.20. Graph of the receiver bender output amplitude as a function of the source bender input square wave voltage. Picks were made of the first trough following the shear wave arrival. The line represents the least squares fitting of a parabola to the four data points.

An example waveform from a compressional bender orientation is shown in Figure 2.21a. The indicated P-wave arrival is interpreted as a compressional wave and the higher amplitude peaks and troughs which follow are interpreted as shear wave arrivals. In order to get an indication of the fourier spectrum of the P-wave only, the received waveform was truncated and cosine tapered at 0.001 s, before the spectral analysis was done. The fourier spectrum of the truncated waveform is shown in Figure 2.21b. The compressional wave arrival time is approximately 650 μ sec. With a separation of approximately 7.5 cm, the loose, dry sand has a compressional wave velocity of 115 m/s.

The bender elements have proven to be a good source and receiver of compressional waves. The amplitudes are not as large as for shear waves, but the faster compressional waves make the picking of first arrivals unambiguous. It also highlights the fact that when the benders are in a shear orientation any compressional waves generated will have a smaller amplitude than the shear waves, making it easier to discriminate the first arrival of the shear waves. For the experiments in the bucket of sand the separation of the elements was not more than 7.5 cm. In order to investigate changes in the first arrival waveform with separation, a sandbox was utilized.

2.4.3 Sandbox Bender Experiment

The bender elements were evaluated in a sandbox in order to determine the effect of bender separation on the received waveform. The sand bucket and sandbox experiments are analogous to using the benders as a probe to determine in situ, shallow shear wave velocities. They proved to be very effective with a source receiver separation as great as 35 cm. A compact waveform propagates from source to receiver with attenuation and dispersion evident in the received waveform at greater distances. Reflections from the surface of the sand or the sides of the sandbox did not seem to be a factor in the experiment.

The sandbox data is shown in Figure 2.22. The data consists of a plot of the received waveforms, at the four separations utilized, with the zero amplitude of each trace plotted at

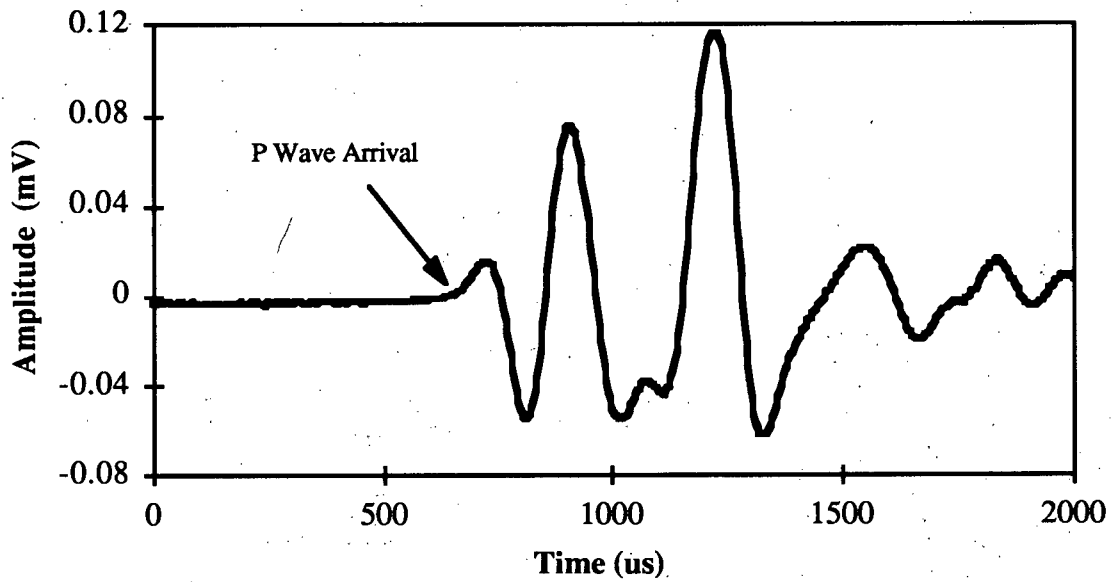


Fig. 2.21a. A waveform from the sand bucket experiment with the benders in an orientation favorable for compressional waves. Approximate separation is 7.5 cm.

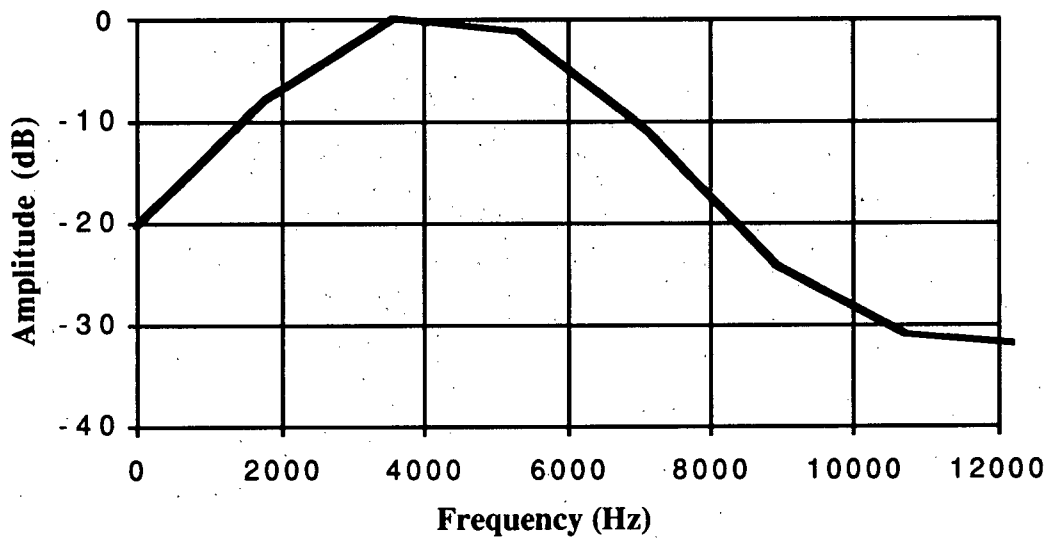


Fig. 2.21b. The amplitude spectrum of the waveform in Figure 2.21a, truncated at 1000 μ s.

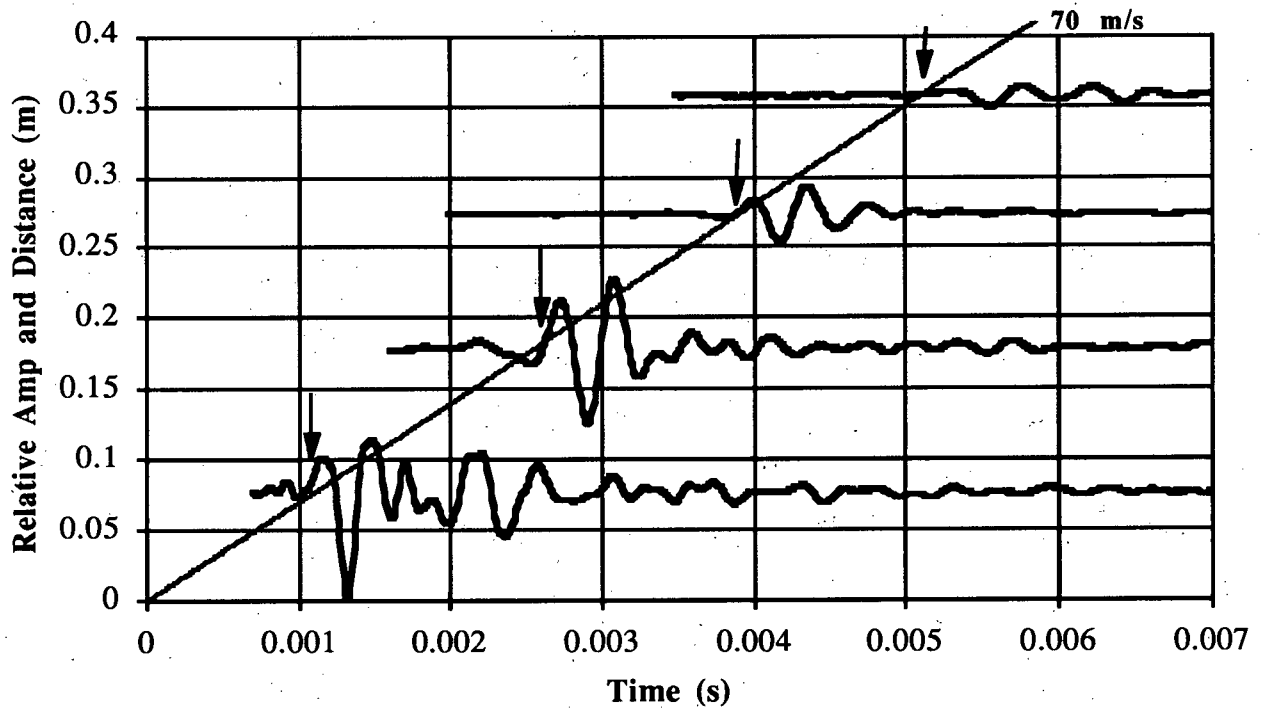


Fig. 2.22. Composite sandbox data, showing the waveforms obtained at the 4 separations. The arrows indicate the interpreted first arrival picks of the shear waves.

the bender tip separation distance. The partly saturated sand in the sandbox resulted in an electrical coupling of the source to receiver (through the capacitive pore fluid), that had the effect of shifting the waveforms in a slow, time varying manner. This shift was removed from the waveforms, before integration into Figure 2.22, by fitting a simple polynomial to the data and subtracting it. The shear waveform is clearly visible, with the proper polarity and general waveform shape, observed in all other tests of the elements. As in the case of the sand bucket, the slight trough preceding the first lobe of the shear arrival is a near field effect associated with compressional wave motion (Yan, 1990).

For these elements the most effective separation seemed to be around 15 to 20 cm, where sufficient dynamic range exists to differentiate the first arrival from the noise and the dominant frequency is reasonably high. The shear wave arrival is interpreted at the zero crossing preceding the first large peak and is shown in Figure 2.22 by the arrows. A line with a slope of 70 m/s and passing through the origin, intersects the interpreted onset of the shear waveform, consistently at all source-receiver separations. This confirms the use of the zero crossing of the compact waveform as a good measure of first arrival velocity.

The data obtained from the sandbox experiment used 0.5 in (1.3 cm) bender elements. The manufacturer specifications for the elements indicate they can withstand 200 V DC. The maximum voltage applied in the sandbox was 3 V. The sand bucket experiments indicated that the benders can be driven at higher voltages which results in a higher amplitude received waveform. The relationship is not linear, but there will always be an increase in bender flexure with applied voltage. The higher amplitude shear waves will propagate further than the lower amplitude shear waves before the signal becomes obscured by the noise. This indicates that the benders used in this thesis can be driven at a higher voltage to propagate shear waves further than 35 cm. The range will still be limited, however, and will probably be less than one meter. A larger bender will generate a lower frequency shear wave that will not be attenuated as rapidly as a higher frequency shear wave and will propagate further. The larger benders will require larger driving voltages, which will necessitate specialized

instrumentation. It is estimated that even with a larger bender element the effective range in cohesionless sediments, due to the high attenuation characteristics, will be in the 10's of meters.

2.5 Summary

Simple experiments have demonstrated the usefulness of the bender elements for geophysical applications. The measurement of elastic wave velocities, both shear and compressional, can be used in the laboratory to investigate the fundamental physics of cohesionless sediments. The sand bucket and sandbox experiments demonstrate that the benders may be useful as a probe for determining velocities in soils.

The utilization of bender elements as probes in unlithified sediments is a powerful tool that can be used to obtain in situ measurements of elastic wave velocities. The in situ velocities are useful for calibrating deeper seismic data and for geotechnical applications, where in situ shear wave velocities give an indication of sediment stability, and in situ compressional wave velocities can be used to evaluate saturation. The elements are inexpensive and straight-forward to manufacture. The electronics required to operate the benders is simple. The bulky nature of the oscilloscope and function generator make them impractical for field application, however, compact instrumentation can be developed. The benders must be inserted into the material to be investigated. This limits their application to sediments which have not been lithified.

The ability to transmit shear waves within the sandbox indicates that the bender elements may be usable as a source and receiver for shallow reflection surveys. A compact pulse generated by the source will propagate through a layered medium, reflecting, transmitting and refracting at interfaces. The receiver bender will pick up any waves which return to the surface. The result is directly analogous to reflection seismic profiling as used by crustal seismologists and the oil exploration industry.

Chapter 3

THE MEASUREMENT OF VELOCITIES IN A COHESIONLESS SAND PACK USING A CONFINING PRESSURE CELL

3.1 Introduction

The measurement of elastic rock properties in the lab has been beneficial to understanding the field response of processed seismic data. In the laboratory the fundamental physics of materials can be examined using controlled experiments with limited variables. The measurement of high frequency (100's of kHz) compressional and shear wave velocities in rocks has been routinely carried out for many years (Hughes and Cross, 1951; Goertz, 1994). The study of unlithified sediments is becoming important for environmental applications. The research challenge is to develop laboratory techniques capable of measuring elastic wave velocities in unlithified materials. Of particular interest is the effect that pore fluid has on the elastic wave velocities.

The elastic wave velocities in any homogeneous and isotropic material are a function of the bulk and shear moduli and the density. The shear wave velocity, V_s , is given by

$$V_s = \sqrt{\frac{\mu}{\rho}} \quad (3.1)$$

where μ is the shear modulus and ρ is the density. The compressional wave velocity, V_p , is given by

$$V_p = \sqrt{\frac{K + \frac{4}{3}\mu}{\rho}} \quad (3.2)$$

where K is the bulk modulus. The shear modulus is a measure of the rigidity of the material

to a shearing force and the bulk modulus is a measure of the compressional rigidity of the material. A change in shear modulus will affect both compressional and shear wave velocities, while a change in the bulk modulus will only affect the compressional wave velocity. It is the effect of pore fluid on the shear modulus that is of primary interest in this chapter.

The monitoring of fluid distribution is a key element in contaminant investigations and production from hydrocarbon reservoirs. Seismic techniques provide remote, non-destructive methods for monitoring fluid distribution. The propagation of seismic energy is governed by the elastic properties of the subsurface. This includes the rock and fluid properties. The fluid properties which have a significant effect on elastic wave velocities are compressibility, density and viscosity. The fluid compressibility will only affect the compressional wave velocity. A decrease in compressibility of the pore fluid (e.g. saturating an air filled porous medium with water) will increase the bulk modulus and the compressional wave velocity will increase as a result. The fluid density will affect both the compressional and shear wave velocities. Compared to an air filled porous medium, a water saturated medium will have a greater mass and hence a greater density. The increased density results in a decrease in both compressional and shear wave velocities, that can be seen in equations (3.1) and (3.2). The fluid viscosity has an indirect effect on the compressional and shear wave velocities.

Variations in fluid viscosity are significant in a number of subsurface situations. Steam injection during heavy oil production causes large changes in viscosity and there is a viscosity contrast between groundwater and contaminants, or their biodegraded products, at contaminated sites. While the traditional approach has been to assume that shear waves are insensitive to fluid content, some recent theoretical research by Dvorkin et al. (1994) indicates that we have been greatly under-estimating the information on fluid content contained in shear data.

Dvorkin et al.'s theoretical work suggests that there is a link between fluid viscosity

and the bulk and shear moduli that results from the movement of pore fluids when elastic waves propagate through a porous medium. Dvorkin et al. (1994) consider both the compressional and shear wave velocities and it is assumed the porous medium is fully saturated.

Experimentally, it is difficult to saturate a sand pack, and eliminate all air bubbles to obtain full saturation. The presence of small air bubbles in the saturated porous medium will have a significant effect on the bulk modulus and the compressional wave velocity. The variations in compressional wave velocity, with saturation, are large enough that variations due to changing viscosity will be difficult to identify experimentally. The shear wave velocity is linked to saturation by the changing density, a bulk property that will not change significantly if small air bubbles are present. The experimental considerations and the traditional assumption that fluids will not affect the shear modulus are the main reasons the change in shear modulus with viscosity is the subject of this investigation.

The research challenge is to develop an experimental apparatus capable of measuring the changes in shear modulus with viscosity and to support the theoretical work. An apparatus has been developed using bender element technology that enables the measurement of shear wave velocities in cohesionless material. The confirmation of a link between shear modulus and fluid viscosity will have a significant impact on the future development of seismic surveys for both production monitoring and contaminant investigations.

3.2 The Effect of Fluid Viscosity on Elastic Wave Velocities

Recent theoretical work (Dvorkin et al., 1994) suggests a link between fluid viscosity and the compressional and shear wave velocity. This link results from a frequency dependent effect related to the movement of pore fluids when a seismic wave passes through a porous medium. The location of the viscous fluids within the pores is important in the theoretical development.

All porous media have a distribution of pores which vary in their aspect ratio. The

aspect ratio is the ratio of the short to long dimensions in a two dimensional cross section of a pore. The pores with a small aspect ratio have crack-like geometries and the pores with an aspect ratio close to 1 have spherical geometries. In general the crack-like pores are very compliant and the spherical pores are rigid when subjected to compressional or shear stresses. For a material consisting of spherical grains, coated with viscous contaminant, the crack-like pores are represented by the narrowing pore space where the grains come into contact (Figure 3.1). In the presence of pore fluids, the crack-like pores transmit significant stresses to the fluid, thereby setting up pressure gradients within the fluid. The pressure gradients result in fluid flow, which follows the local flow model suggested by O'Connell and Budiansky (1974, 1977) and Mavko et al. (1979).

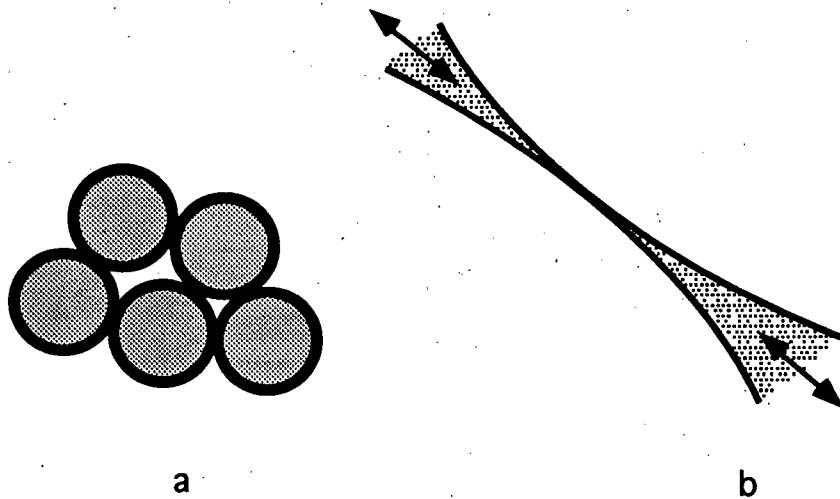


Fig. 3.1. Diagrams illustrating the crack-like porosity present in a packing of spherical grains coated with contaminant. a) Spherical grains coated with contaminant. b) Local flow at grain contacts.

The local flow model is frequency dependent. At relatively low frequencies the pore fluid flows and the pressure gradients dissipate. At relatively high frequencies the pore fluid does not have time to move (Mavko and Jizba, 1991). The pore fluid in this case is referred to as "unrelaxed". The unrelaxed fluid acts as a rigid component of the contact area that

increases the rigidity of the contact and thus the medium as a whole. The higher the viscosity of the pore fluid, the more difficult it is for the fluid to flow and for pressure gradients to dissipate. A significant aspect of the theory is that the viscous fluid must lie within the most compliant pore spaces. This frequency/viscosity dependence is shown in Figure 3.2, which illustrates that even at frequencies as low as 100 Hz there are significant variations in both compressional and shear wave velocities, associated with viscosities of 1000 to 10 000 mPa.s in the saturating fluid. These figures are representative of the characteristics expected for water saturated Navajo sandstone with viscous fluid in the crack-like pores. The relationship changes for a material consisting of glass beads.

Dvorkin et al. (1994) also compute the compressional velocity versus frequency and viscosity for coated glass beads. This relationship is shown in the graph of Figure 3.3. It is assumed that the glass beads are coated with a uniform layer of viscous fluid, that places the viscous fluid in the crack-like pores. In this case the changes in compressional wave velocity, for viscosities ranging from 1000 to 100 000 mPa.s, are not significant until frequencies of 10 to 100 kHz are reached. Based on the similarities between the compressional and shear wave velocities as a function of viscosity and frequency in Figure 3.2, it is assumed that the similarities can be extended to the coated glass beads. The shear wave velocity in the coated glass beads should also vary with viscosity and frequency. The differences between Figure 3.2 and Figure 3.3 are attributed to differences in the pore geometries between Navajo sandstone and a glass bead pack. The spherical nature of the glass beads should result in a reduction in the number of compliant pore areas, compared to the sandstone. For a real sediment where a variety of grain sizes and shapes can be expected the number of crack-like pores will be greater and the frequency at which a viscosity effect can be identified should be lower.

Dvorkin et al.'s theoretical development has definite implications for the laboratory identification of a dependence of shear wave velocity on viscosity. For a cohesionless sand

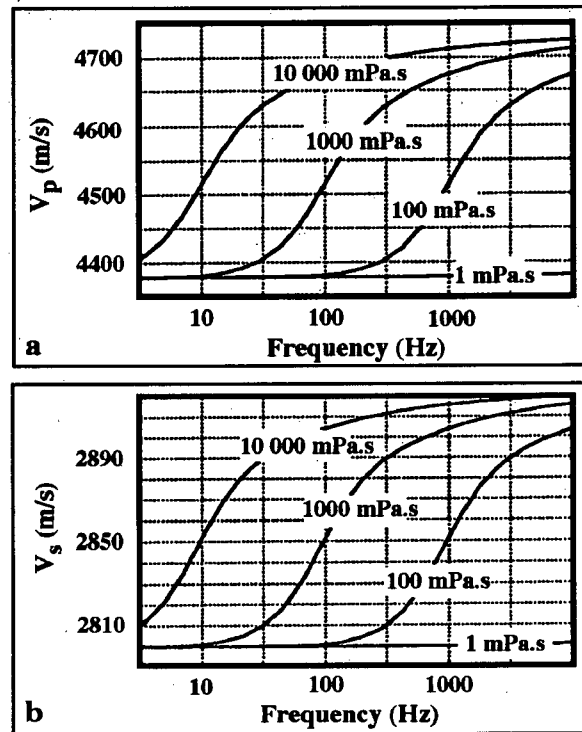


Fig. 3.2. Graphs of (a) compressional wave velocity and (b) shear wave velocity as a function of frequency for water saturated Navajo sandstone with viscous fluid in the crack-like pores. The viscosity of the viscous fluid is indicated on the graphs (After Dvorkin et al., 1994).

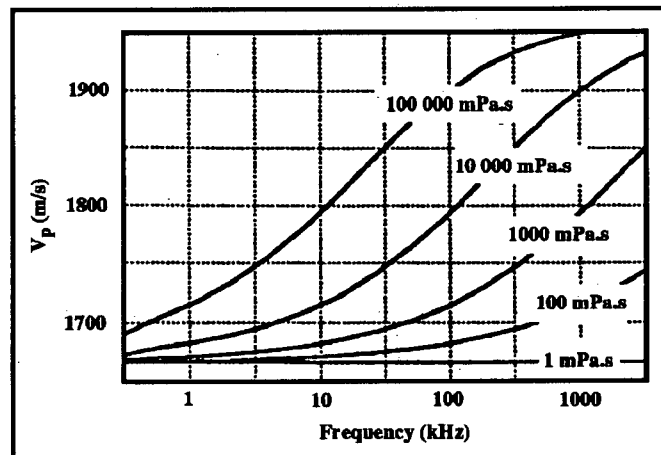


Fig. 3.3. Compressional wave velocity as a function of frequency in a cohesionless packing of water saturated glass beads. The glass beads are coated with viscous contaminant with the viscosity of the contaminant indicated on the graph (After Dvorkin et al., 1994).

the viscous fluid must coat the sand grains as completely as possible, ensuring that the fluid gets into the crack-like pore spaces. The wetting nature of the viscous fluid will also affect how easily it coats the sand grains. The presence of water on the grain surfaces will prevent a non-wetting fluid (such as silicon oil) from completely coating the sand grains. The experimental challenge is thus to reduce the amount of any wetting phase present on the sand grains and to ensure that the viscous fluid reaches the crack-like pores.

3.3 The Stress State of a Sand Pack Under Uniaxial Compression

An understanding of the stress state of a sand pack under uniaxial compression is critical to understanding the experimental results contained in this chapter. Variations in the stress state have a significant effect on the compressional and shear wave velocities. The analysis examines the force balance of a sand pack under uniaxial compression, with and without the inclusion of a frictional force on the walls of the cylinder. The frictionless case will be analyzed using an empirical relationship developed by Yu and Richart (1984) that will then be used as a basis for making conclusions about the stress state when friction is present.

A diagram illustrating the forces acting on a sand pack under uniaxial compression is shown in Figure 3.4. The cylinder is subjected to an axial force F_a which results in an axial stress $\sigma_a = F_a/A$ on the sand pack adjacent to the piston. The force balance will be considered using two scenarios, one without the frictional force on the sides of the cylinder and the other which includes the frictional force.

Neglecting the presence of the friction on the walls of the cylinder, and assuming a very rigid cylinder relative to the sand pack, the sand will be under an uniaxial or confined compression. The axial stress will be the same throughout the sand pack and equal to σ_a (i.e. $\sigma_a = \sigma_c$). The sand pack will initially respond elastically to the increased stress. The elastically deformed and loaded sand grains will have stiffer grain contacts, resulting in an increased overall rigidity and therefore a higher shear wave and compressional wave velocity. The

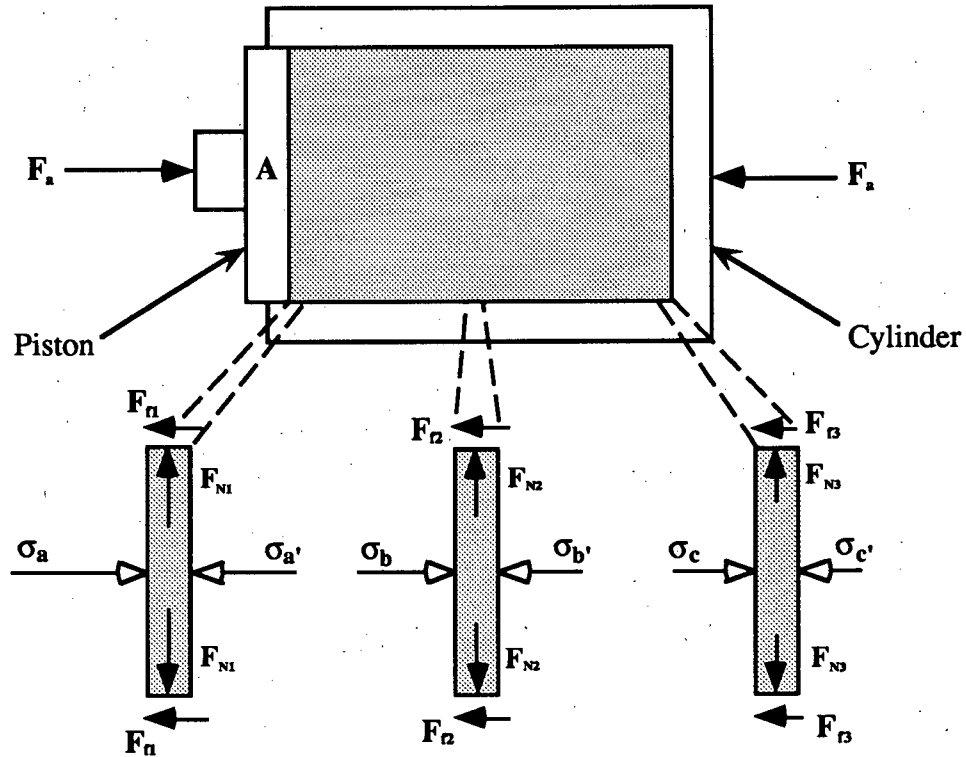


Fig. 3.4. Diagram of the force balance on a sand filled cylinder, under uniaxial compression. The area of the piston in contact with the sand pack is A .

increased stress will also cause the sand grains to move into a closer packing, resulting in a reduction in the void ratio. The closer packing will increase the number of grain to grain contacts, and thus the compressive and shear rigidity will increase. The moduli of the sand pack will increase due to the increased confining stress and will also increase due to the closer packing of the sand.

The sand under uniaxial compression will be in an anisotropic stress state with the axial stress greater than the lateral stress (Lambe and Whitman, 1979, 127). The ratio of lateral to axial stress is referred to by geotechnical engineers as K_0 , and is typically in the range 0.3 to 0.5, for normally consolidated soils (Thomann and Hryciw, 1990). The stress in the lateral direction will affect the shear modulus seen by elastic shear waves propagating in an axial direction, because the lateral stress is in the direction of particle displacement. Yu and Richart (1984) established an empirical relationship relating shear modulus to the void

ratio and average stress of the sand pack. This relationship is a modified form of the expression arrived at by Hardin and Richart (1963), that considered the isotropic stress state only. The expression for shear modulus, G_0 , is

$$G_0 = \frac{A}{F(e)} (P_a)^{0.5} \left[\frac{\sigma_a + \sigma_l}{2} \right]^{0.5} \quad (3.3)$$

where P_a is the atmospheric pressure, σ_a and σ_l are the axial and lateral stresses, and for angular sand $A=326$ and $F(e)$ is given by

$$F(e) = \frac{1+e}{(2.97-e)^2} \quad (3.4)$$

where e is the void ratio.

The inclusion of the frictional force results in a variation in the axial stress through the sand pack. The frictional force is a function of the normal force on the walls of the cylinder, that is designated F_N in Figure 3.4, and the coefficient of friction. This normal force results from the lateral stress acting on the surface area of the cylinder. The frictional force acts to reduce the stress transmitted through the sand pack, thereby reducing the axial confining stress at the bottom of the cylinder. The reduced axial stress will also reduce the lateral stress and thus the frictional force will also decrease towards the bottom of the cylinder. The lower axial and lateral stresses will result in a smaller shear modulus that is apparent from equation (3.3).

3.4 The Effect of Water Saturation on a Sand Pack Under Uniaxial Load

The addition of water to a sand pack will have a number of effects; the pore fluid pressure will oppose any change in applied stress, the water will affect the grain contacts and the anisotropic stress state will change. Each of these effects will be discussed in greater detail.

The pressure of the water on the surrounding sand grains will act to oppose an increase in applied stress. The matrix will see a reduced stress referred to as the effective stress. The effective stress σ_e was first detailed experimentally by Terzaghi (1923) and is given by the expression

$$\sigma_e = \sigma - \mu \quad (3.5)$$

where μ is the pore pressure and σ is the applied stress. When a stress is applied to a sand pack and the water is allowed to drain from the sand, the water will flow and the pore pressure will not increase above hydrostatic. This is referred to as a "drained" situation. In the drained situation the effective stress will increase by the same amount as an increase in applied stress. Conversely, where the water is not allowed to drain, the confinement of the water will result in an increase in fluid pressure, when the confining stress is increased. This is referred to as an "undrained" situation. In the undrained situation the increase in pore pressure will offset the increase in applied stress and the effective stress will remain constant. The actual draining process occurs due to the establishment of pressure gradients within the fluid; these gradients will equilibrate by fluid flow if an opening is provided to atmospheric pressure. In all experiments with the confining pressure cell, an opening was provided to atmospheric pressure, when a fluid was present in the sand and the axial stress was increased.

The water will also affect the grain contacts. A small amount of water in the grain contact region will make the contacts less rigid and result in a reduction of the shear modulus. This affect was noticed experimentally by Hardin and Richart (1963), for Ottawa sand, where a reduction in shear modulus of 15% was noted for saturations as low as 1.4%. The reduction of shear modulus at low saturations is analogous to that seen by Goertz (1994) in samples of Berea 100 and Berea 300 sandstone. The experiments carried out by Hardin and Richart (1963) on crushed (angular) quartz sand, however, showed no reduction in shear modulus with saturation. This can be explained because the angular grains are more likely to

have interlocking contact regions, which will be affected less by the presence of water.

The change in the stress state of a sand pack will have a definite effect on the shear modulus. An increase in the lateral stress will increase the shear modulus seen by a shear wave traveling in the axial direction. This results because the lateral stress acts in the direction of particle displacement. It is difficult to quantify the variation in lateral stress due to saturation because of the anisotropic stress state of the cell, but in general the lateral stress is most likely to increase, making the stress state closer to a hydrostatic (isotropic) stress state.

3.5 Experimental Procedures

3.5.1 Apparatus Description

An apparatus has been designed to enable the measurement of elastic wave velocities in a cohesionless sand pack, with varying confining stress. The apparatus consists of a Plexiglas cell with fluid saturation and vacuum ports, and the instrumentation to generate pulses and measure the weak voltages and time delays associated with the propagating waves. A diagram of the apparatus is shown in Figure 3.5. A key design feature of the apparatus is the utilization of bender element technology which is outlined in Chapter 2.

The cell consists of a 19 cm long Plexiglas tube with an inside diameter of 8.3 cm and a wall thickness of 0.6 cm. A sturdy 1.9 cm Plexiglas base is epoxied to one end of the tube, with a recessed hole centered on the outside to accommodate the load cell button. A 1.3 cm wide by 1.9 cm thick Plexiglas skirt is epoxied to the top of the cell which has four tapped holes in it to hold the lid in place. Two brass valves are located at the top and bottom of the cell, at opposite sides, to allow for the pulling of a vacuum and the attachment of a fluid reservoir. Three holes are drilled in the side of the cell, perpendicular to the valve locations, to accommodate the Swagelok bulkhead feedthroughs of the bender assemblies. The holes are drilled to provide two possible source/receiver bender tip separations of 5 cm and 10 cm.

The hole closest to the bottom is used for the receiver bender assembly and is on the opposite side of the cylinder. This provides the longest possible travel path for vibrations leaking from the source bender, through the Plexiglas to the receiver bender. To provide acoustic damping of any leakage signal, the bender assemblies have a silicon gasket and are held in place with rubber o-rings. A Swagelok bulkhead feedthrough with a sealed plug is used in the hole without a bender assembly.

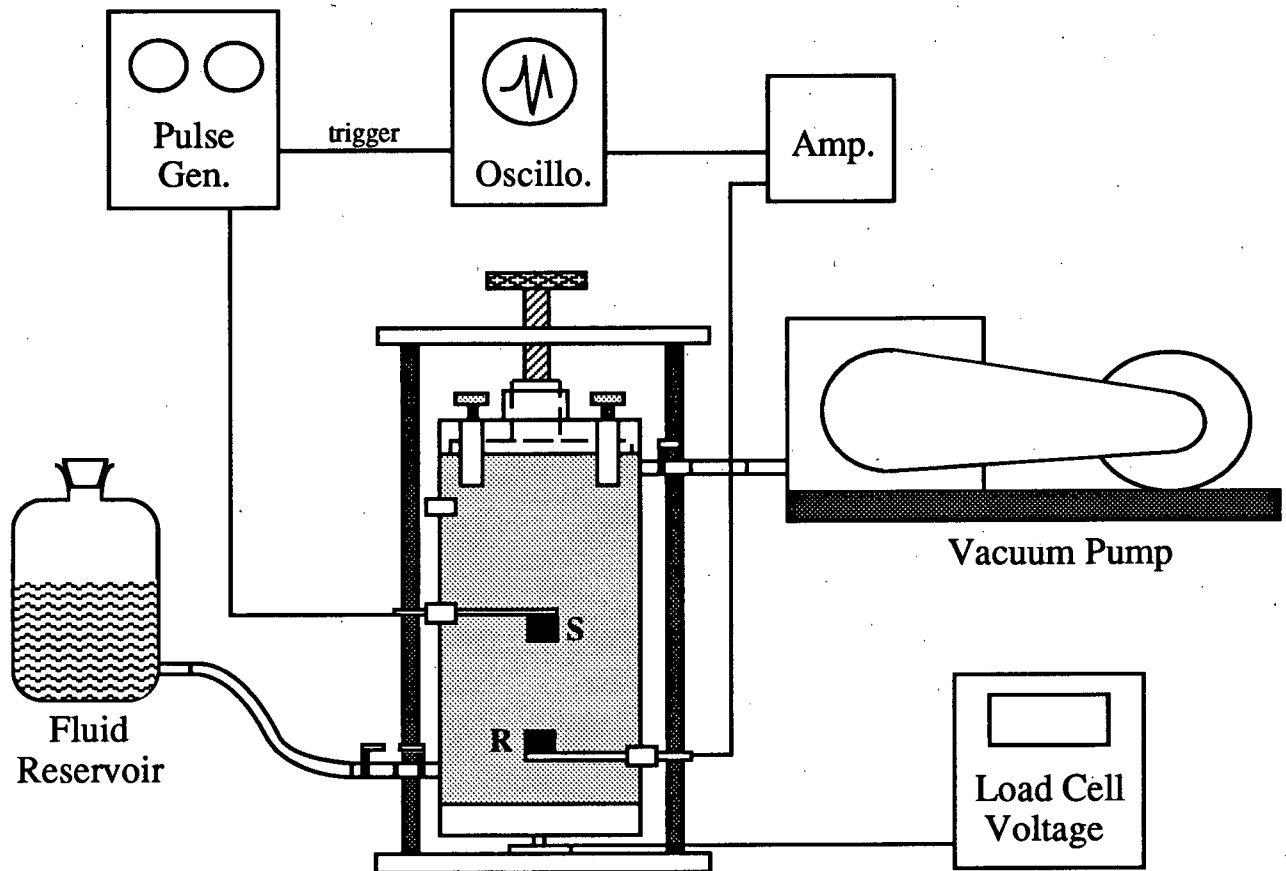


Fig. 3.5. Diagram of the confining pressure cell, with bender elements (designated S and R), mounted in the loading apparatus with the laboratory equipment used to saturate the sand pack and measure elastic wave velocities.

The lid for the cell has four holes to match the skirt of the body, and a recessed slot to accommodate a flush mount piston made of rigid PVC plastic. An o-ring in the sealing face of the lid provides a vacuum tight seal when the hold down screws are tightened. The piston

push rod follows a guide in the lid which has two o-rings to provide a vacuum seal. When assembled the cell is capable of holding a vacuum of 50 microns .

The source bender element is connected to an IEC F33 function generator, which is capable of putting out a 20 V peak-to-peak square wave with a rise time of 60 nsec. The receiver bender has its individual leads attached through the shielded center conductor of coax cables to the differential inputs of a Stanford Research Systems SR560 voltage preamplifier. The use of the differential inputs allows the subtraction of any coupled noise developed in the cables, produced by overhead fluorescent lighting and nearby transformers. The amplifier also allows the bandpass filtering of the signal. A 300 Hz to 1 MHz bandpass filter was used with 6 dB/octave slopes on the high and low ends. The output of the amplifier is sent to a Tektronix TDS 420 digital oscilloscope, where the signal can be averaged to further reduce any noise. The oscilloscope is triggered by the function generator to establish the zero time for the traces. The oscilloscope is also capable of storing up to four signals in memory. This allows for the transfer of the data to a Macintosh Quadra computer using the Labview software package.

3.5.2 Measurement Procedure

The purpose of the experiments is to measure variations in velocity that are solely due to changes in the saturating fluid. As such it is critical that all other parameters affecting the experiment remain constant from one experiment to the next. The key parameters which have been identified are sand packing, loading history, and fluid saturation. Each parameter will be discussed in greater detail.

The sand packing determines the matrix through which the shear waves will propagate. In order to ensure uniformity the following procedures were carried out:

1. Using a glass funnel with a 0.397 cm opening, and holding the funnel tip at the top of the cell, the cell was filled by poring sand from the funnel to the base of the

- lowest bender (approximately 2.5 cm of sand).
2. Using a rotary pad sander on the bottom of the cell, the cell was agitated for 2 min.
 3. The cell was filled, using the funnel, to the top of the middle bender assembly hole (on the side of the cell).
 4. The cell was agitated for 5 min.
 5. The cell was filled to the top of the upper bender assembly hole.
 6. The cell was agitated for 5 min.
 7. The cell was filled to the top, with a 1 cm high mound of overfill.
 8. The cell was agitated for 5 min.
 9. A straight edge (plastic ruler) was used to level off the top of the cell.

The use of the funnel to pore sand from an opening of fixed diameter and uniform drop height is a dry pluviation technique commonly used by geotechnical engineers to prepare repeatable samples. The filling and densifying (agitating) of the sand pack in stages was required in order to reduce the porosity, in a repeatable fashion. The mass of sand which could be placed in the cell was repeatable to within 1.5%, and the porosity was repeatable to within 0.5%.

All measurements were made with the cell in a horizontal orientation. This was done to ensure that the stress on the sand between the benders did not change due to differential overburden stress. In order to eliminate any excess water which may have accumulated on the sand, the sand was oven dried overnight and a vacuum was applied to the packed cell for two hours, before any measurements were made. The starting waveform of the receiver bender element and the initial velocity varied with time and experiment, illustrating the sensitivity to low confining stresses. In order to obtain a repeatable waveform, it was deemed necessary to apply a confining stress to the sand pack.

The axial stress applied to the cell varied from 0 to 200 kPa that is analogous to the overburden pressure in the upper 25 m of the subsurface. A series of loading cycles was used

in the application of the axial stress to the cell. Initially the dry sand was loaded in small stress increments up to 200 kPa. After each stress increment, the sand pack strain resulted in a reduction of the stress over time. The loading screw was tightened a number of times to maintain the stress at a particular value. After approximately 5 min, the change of stress with time was minimal and a measurement of the travel time of the elastic wave was made. For each measurement of elastic wave velocity, up to an axial stress of 200 kPa, the sand pack was first allowed to reach an equilibrium with respect to the applied load.

The stress was then reduced to 50 kPa and a vacuum was applied to the sand pack. The sand was then reloaded to 200 kPa and a measurement of the velocity was made to see how much the velocity varied from the previous measurement at an axial stress of 200 kPa. After two cycles the variation in velocity was usually within 1%. The confining stress was then lowered to 50 kPa, the cell was turned upright, the fluid reservoir was connected to the saturation port, and a vacuum was applied to the sand.

To reduce fingering of the fluid as much as possible, the cell was always saturated from the bottom up. While the fluid was flowing into the cell, the vacuum was left on, effectively removing as much of the residual air as possible. When the fluid reached the level of the vacuum port, the valve was shut off and the fluid was allowed to fill the rest of the cell. Using water as the saturating fluid, the saturation typically ranged from 0.995 to 1.000. This fluid saturation technique seems to result in no noticeable air bubbles within the sand pack, thereby ensuring the fluid reaches a significant number of crack-like pore spaces.

The porosity of the sand pack was determined for each experiment. The volume of the cell was measured by weighing the cell empty, then plugging all portions of the cell, that sand will not occupy, and filling it with water. Knowing the density of water, the change in mass gives the volume. This volume was 1.041 l. A representative sample of Lane Mountain sand, of known mass, was then placed in the helium porosimeter to measure the volume, and thus the density of the sand was determined. The density of the sand was 2.659 g/cm³. When the cell was filled with sand the mass of sand put into the cell was measured and the sand

density determined the volume of sand in the cell. The difference between the sand volume and the cell volume gave the pore volume and thus the porosity was determined.

The porosity was also determined by weighing the cell before and after saturation, to determine the amount of fluid contained in the sand pack. With no air bubbles in the fluid, the fluid volume will equal the pore volume, and thus the porosity can be determined, without having to know the sand density. In all water saturation experiments, where no air bubbles were evident in the saturated cell, the pore volume determined using the two techniques was always within 0.5%. It was therefore assumed that the average saturation could be determined by taking a ratio of the saturated pore volume to the pore volume computed from the sand density.

The fluid which was used for the viscosity experiment is Dow-Corning 200 fluid, and Union Carbide L-45 fluid. The fluid is also called polydimethylsiloxane or silicon oil and consists of silicon-oxygen chains with methyl side groups. The longer the chain, the higher the viscosity. The silicon oil had kinematic viscosities ranging from 10 to 10 000 mm²/s. The chemical properties of each fluid are very similar, making the changes in viscosity the key variable. The specific gravity of the silicon oil was 0.93 for the 10mm²/s oil and 0.97 for the oils with other viscosities.

3.6 Discussion and Results

The Plexiglas cell was used to measure both compressional and shear wave velocities using the first arrivals of the received waveform. Due to the limited size of the cell, the received waveform consisted of a direct arrival as well as arrivals from reflections and refractions from the cell walls. These multipath arrivals all arrive later than the direct arrival because the separation of the elements represents the shortest path through the sand. The cell was filled with sand and a number of fluids (air, water and silicon oil) were used to saturate the sand pack. Each fluid has a characteristic response which is attributable to the damping and electrical properties of the fluid. A series of experiments was carried out using dry and

saturated sand at varying confining pressures. Both compressional and shear wave orientations of the bender elements were utilized.

3.6.1 Compressional Waves in Distilled Water

In order to test whether the bender arrangement within the cell is suitable for measuring elastic wave velocities, the cell was filled with distilled water, for which the compressional wave velocity as a function of temperature is well known. The benders were mounted perpendicular to the cell axis to favor the propagation of compressional waves between the elements. The type of waveform which results from such an experiment is shown in Figure 3.6a. The waveform is characterized by a sharp onset and a cluster of relatively high amplitude peaks and troughs. This cluster of arrivals appears to be very similar to the shear "wavelet" identified in the sand bucket experiments detailed in Chapter 2. Another series of arrivals at approximately $65\mu\text{s}$ also has the same wavelet shape, but is inverted in polarity. This other arrival is interpreted as a refraction from the sides of the cell. The amplitude spectrum of the compressional waveform is shown in Figure 3.6b. The dominant frequency is approximately 300 kHz. The jagged nature of the spectrum is attributed to the short time window used and the "ringiness" of the later arrivals. The sharp onset of the waveform made the picking of the first arrival unambiguous, resulting in very accurate velocity values.

The velocity as a function of temperature is shown in Figure 3.7, along with the published values for distilled water (Becker, 1990). The error bar represents a timing error of $0.04\ \mu\text{s}$ and a bender separation error of 0.2 mm. The error has been computed using the quadrature method outlined by Taylor (1982), which assumes that the uncertainties in the measurements are independent and random. The velocity associated with the bender arrival is within experimental error of the published values, thereby confirming the viability of using benders mounted perpendicular to the cell axis to measure compressional wave velocities.

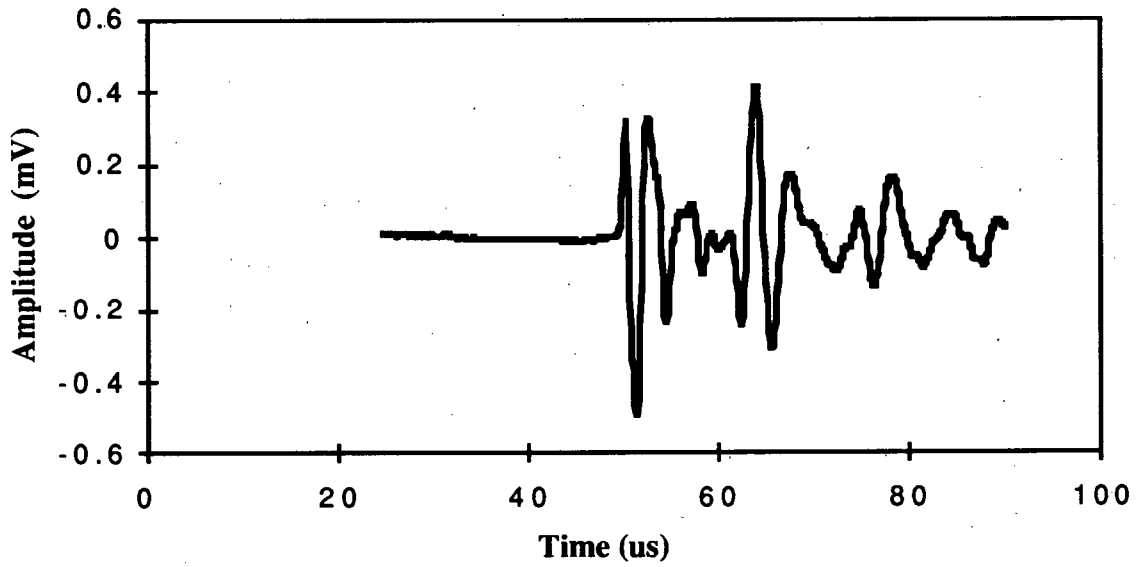


Fig. 3.6a. The received waveform from the confining pressure cell with distilled water in the cell and the benders in an orientation favorable for compressional waves.

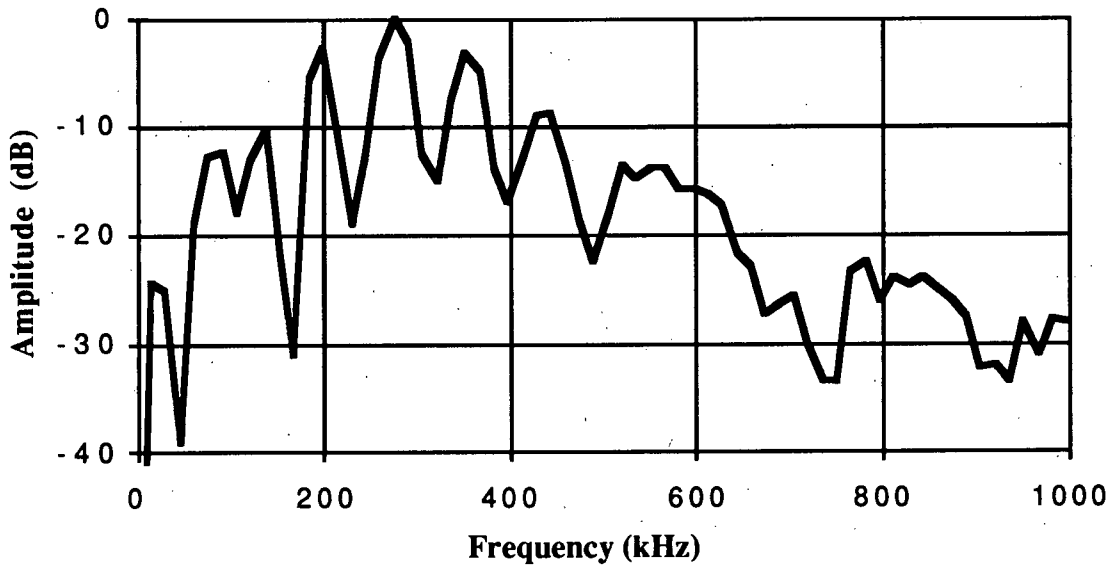


Fig. 3.6b. The amplitude spectrum of the waveform in Figure 3.6a.

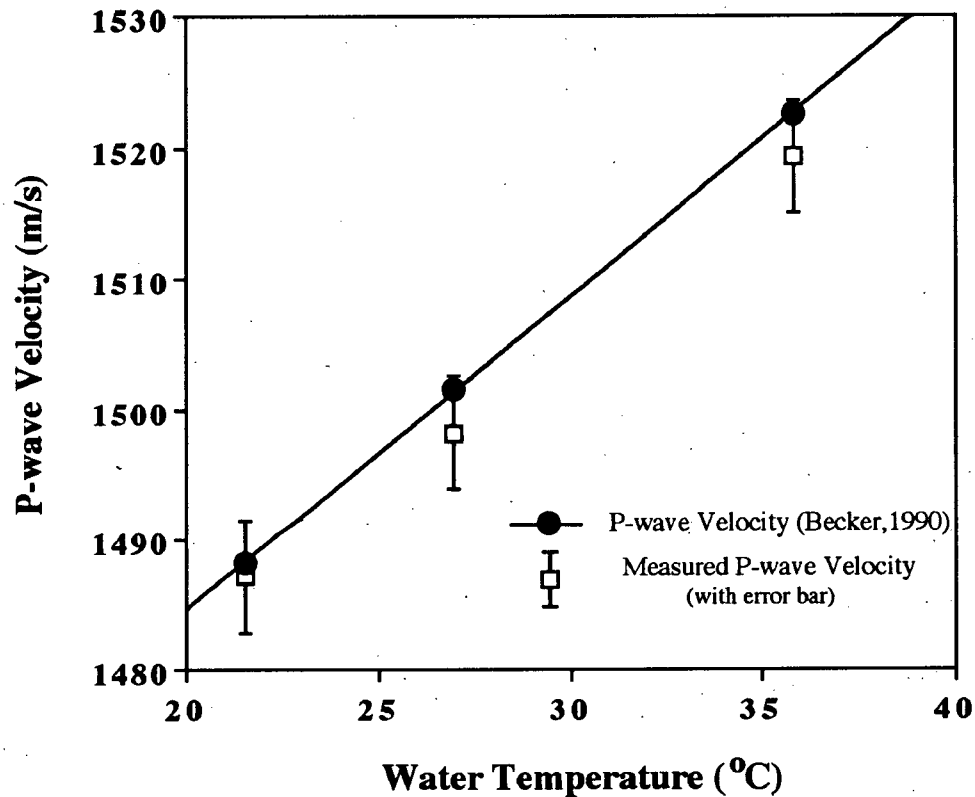


Fig. 3.7. Graph of P-wave velocity as a function of water temperature, measured using the confining pressure cell filled with distilled water and the bender elements in an orientation favorable for the propagation of compressional waves.

3.6.2 Water Saturation Experiments

A series of experiments was carried out using the bender elements in a dry sand pack, which was then saturated with distilled water. The experiments used Lane Mountain sand, which consists primarily of angular quartz grains, although some mica and metallic minerals are also evident. The sieve size 35 to 42 (0.39 to 0.50 mm) was used for all experiments, using the cell. The experiments examined the variation in shear wave and compressional

wave velocities in a dry and saturated sand pack with changing confining pressure.

An example of a shear waveform which has propagated through a dry sand pack in the cell is shown in Figure 3.8a. The waveform consists of a series of distinct arrivals. The first arrival is part of a compact "wavelet" with the same polarity and shape as that identified in the sand bucket experiments (Chapter 2). Following the first arrival wavelet is a series of peaks and troughs, some of which are in the form of the first arrival wavelet. These later arrivals represent the reflections and refractions from the sides of the cell. An example of the shear waveform of the same sand pack after saturation with water is shown in Figure 3.8b. The same arrivals seen before saturation are evident in the waveform, but the arrivals after 800 μs are noticeably reduced in amplitude. This is probably due to reduced coupling of the reflecting waves at the cell walls, due to the presence of water, that will reduce the reflection coefficient and hence amplitude of the received waves. When the sand is saturated the compressional waves will propagate at a higher velocity and at a higher frequency, that will reduce compressional wave interference within the shear waveform.

The data illustrating the measurement of shear wave velocities in a dry and saturated sand pack at different axial stresses is shown in Figure 3.9a. The shear modulus μ is shown in Figure 3.9b and is computed by using the formula

$$\mu = \rho V_s^2 \quad (3.6)$$

where ρ is the density and V_s is the shear wave velocity. The density is obtained from the mass of the sand in the cell divided by the volume of the cell and is assumed to be constant with applied stress. The piston movement, resulting from loading the sand pack from 0 to 200 kPa, was approximately 0.5 mm, which results in a negligible change in density. When the sand pack is saturated, the increased mass of the cell, with constant volume, will determine the saturated density.

The data in Figures 3.9a and 3.9b consists of four loading curves. The first loading

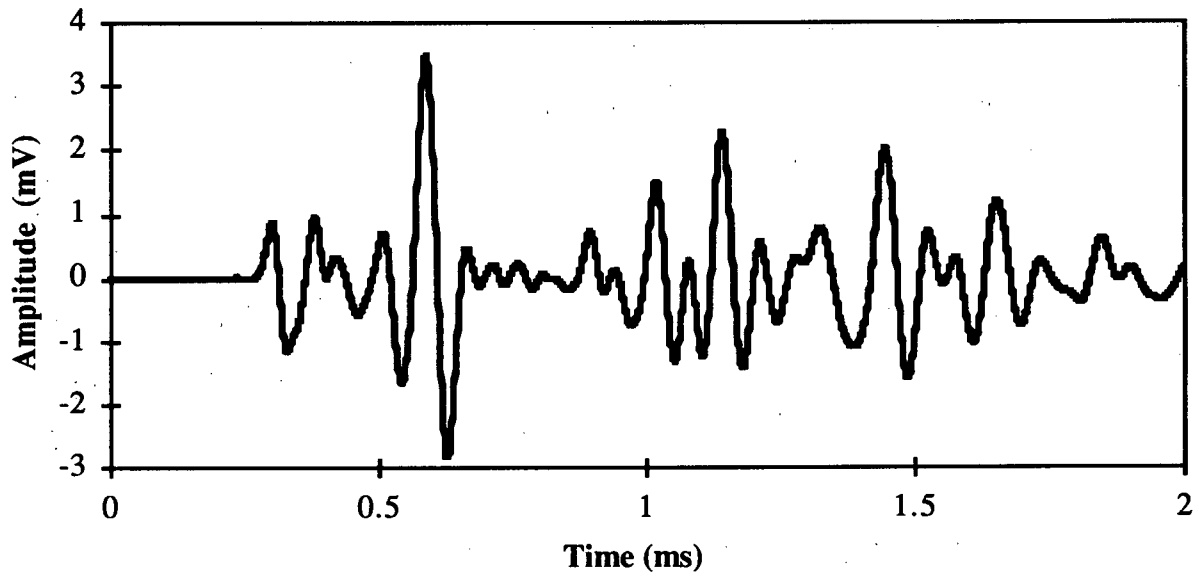


Fig. 3.8a. The received waveform from the confining pressure cell, with benders in an orientation favorable for the propagation of shear waves, and dry Lane Mountain sand packed around them.

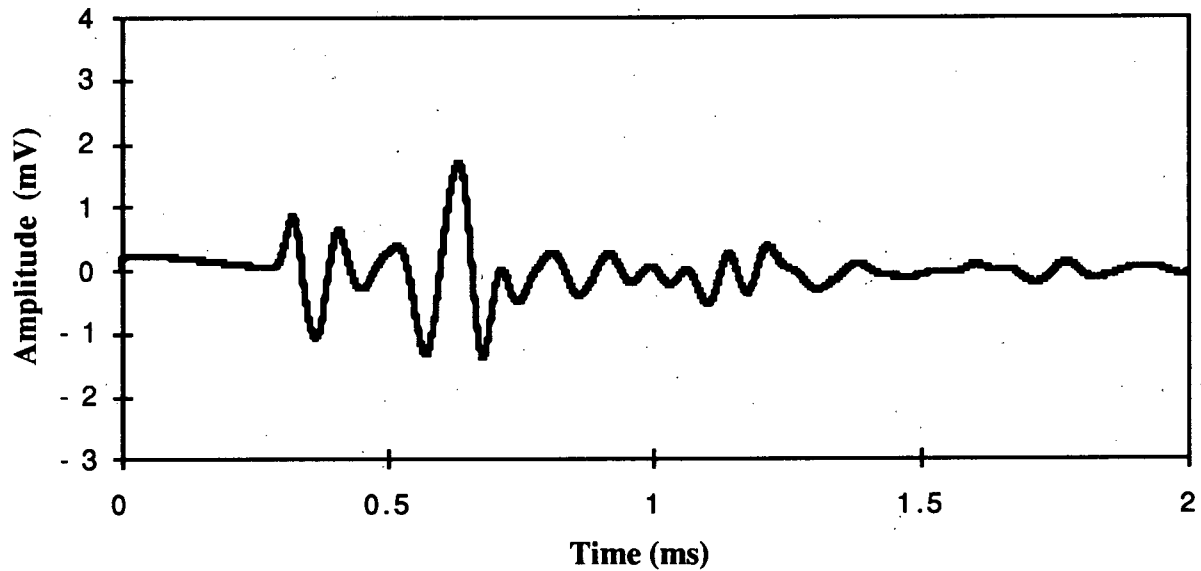


Fig. 3.8b. The received waveform from the confining pressure cell, with the benders in an orientation favorable for the propagation of shear waves, and water saturated Lane Mountain sand packed around them.

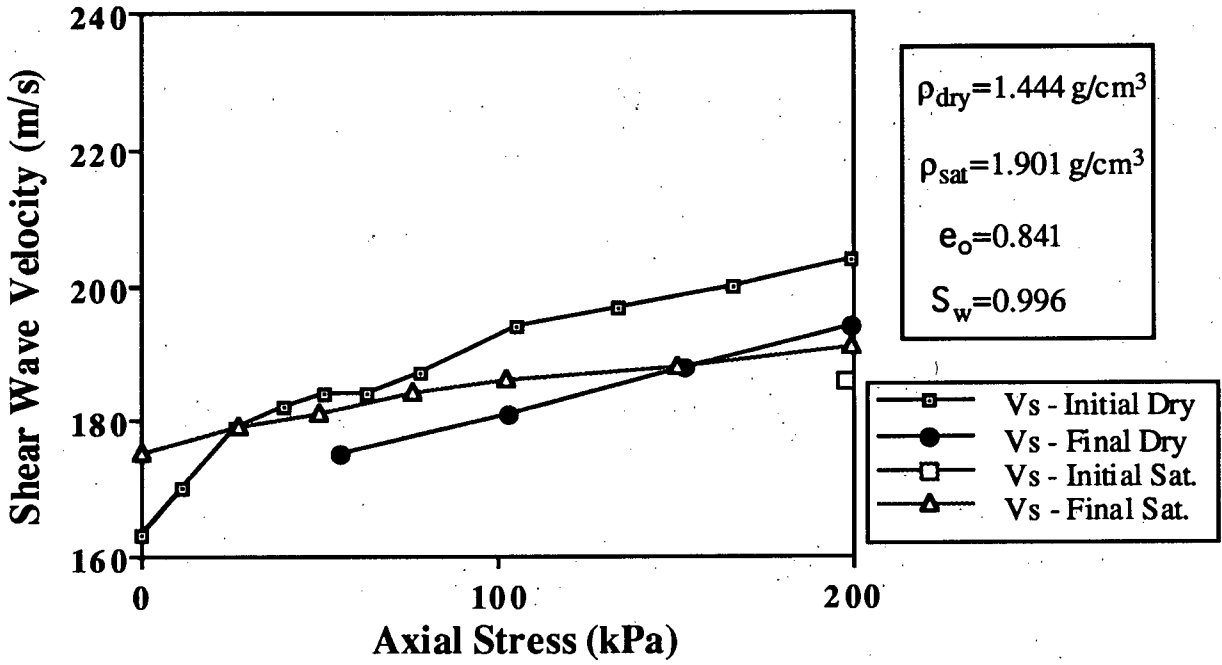


Fig. 3.9a. Shear wave velocity as a function of confining stress for a dry and water saturated Lane Mountain sand pack.

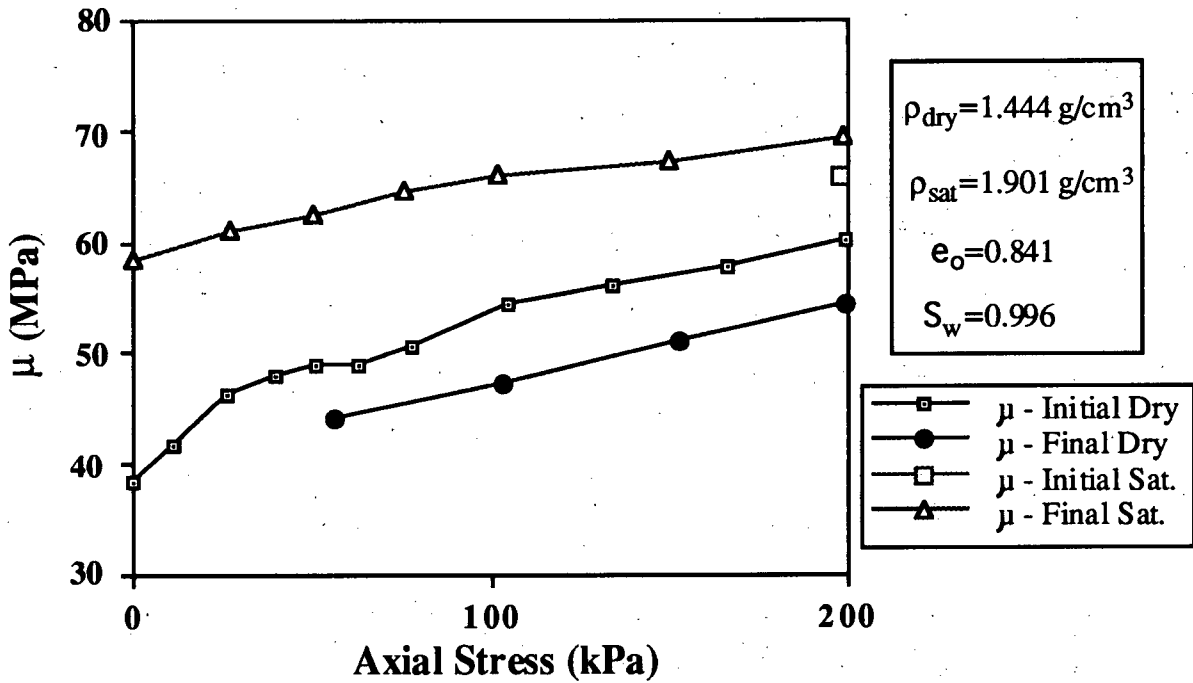


Fig. 3.9b. Shear modulus as a function of confining stress for a dry and water saturated Lane Mountain sand pack.

curve (labeled as "Initial Dry") represents the initial loading of the dry sand pack. The next loading curve (labeled as "Final Dry") represents the final loading of the dry sand pack before saturation. Between the two loading cycles the sand pack has been cyclically loaded two additional times, the purpose being to establish a modulus which does not vary significantly when reloaded. In all experiments using the dry sand (this includes the silicon oil saturation experiments), the shear modulus always decreased when the sand pack was cyclically loaded. This is contrary to what was observed experimentally by Hardin and Richart (1963). The frictional force on the walls of the Plexiglas cylinder is significant and plays a key role in the reduction of the shear modulus with cyclic loading.

When the values of shear modulus shown in Figure 3.9b are compared to those obtained using equations (3.3) and (3.4) the lower axial stress between the bender elements in the confining pressure cell becomes obvious. For an axial confining stress of 200 kPa, a void ratio of 0.841, and an assumed $K_0=0.5$, Yu and Richart's equation gives a shear modulus of 99 MPa, significantly greater than the shear modulus of 58 MPa, measured in the dry sand pack at 200 kPa (Figure 3.9b).

The reduction of the dry sand shear wave velocity with cyclic loading can be explained by considering the frictional force balance in the cell and the change of K_0 with cyclic loading. When a sand is gradually loaded, under uniaxial compression, to a high stress and the stress is then gradually released the K_0 value will be higher upon unloading, at a particular axial stress value (Thomann and Hryciw, 1990). The "locked" grain contacts which enable the lateral stress to be less than the axial stress, upon initial loading, will also be "locked" when the axial stress is released, thereby maintaining some of the built up lateral stress. The increased lateral stress will increase the normal force on the walls of the cylinder and the frictional force will also increase. The increased frictional force will further reduce the stress at the bottom of the sand pack, that will be maintained as long as the K_0 value at a particular axial stress is greater than the previous loading. It is the fact that the sand between the benders is under a reduced axial stress, compared to the previous loading, that causes the

shear wave velocity to decrease. This affect makes it impossible to use the axial stress values, used in the experiments, with any degree of accuracy. It was assumed, however, that the changes in axial stress would still be repeatable from one experiment to the next.

The saturation of the sand pack with water resulted in a final saturation of 0.998. The third loading cycle (labeled as "Initial Sat." in Figure 3.9a and 3.9b) involves the initial loading of the saturated sand pack. In this particular case, only a single data point was obtained when the sand pack was loaded from 50 kPa for saturation to 200 kPa. The modulus has increased, compared to the "Initial Dry" and "Final Dry" data points at an axial stress of 200 kPa. The increase in modulus with water saturation can be explained by a reduction of the frictional force on the sides of the cylinder, by lubrication, and hence an increase in the confining stress seen between the benders. The shear modulus after saturation, at 200 kPa, has a value of 66 MPa, which is still significantly less than the value of 99 MPa, predicted by Yu and Richart's equation. Alternatively, the modulus increase could be a result of an increase in the lateral stress, that will increase the average stress component of Yu and Richart's equation. The final loading cycle (labeled as "Final Sat." in Figure 3.9a and 3.9b) was initiated after the sand pack was completely unloaded (i.e. the cell must be removed from the loading apparatus to measure the mass, and determine saturation). The shear modulus has increased again, which presumably is due to a further change in the stress state. This simple experiment highlights how sensitive the shear modulus is to the stress state of the sand pack between the source and receiver benders at the bottom of the sand pack.

The benders were re-oriented perpendicular to the cell axis to generate compressional waves between the elements. In Figure 3.10a is shown an example of the received waveform. The waveform consists of a small amplitude P-wave arrival and a series of large amplitude troughs which are probably associated with shear waves. The same sand pack saturated with water results in the waveform shown in Figure 3.10b. The electrical coupling

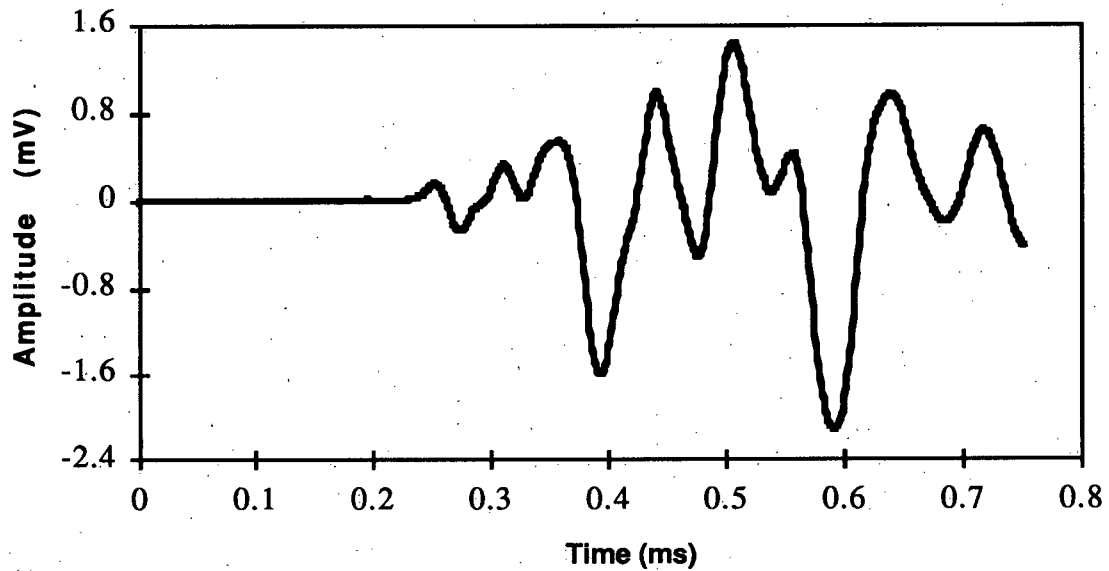


Fig. 3.10a. The received waveform from the confining pressure cell, with benders in an orientation favorable for the propagation of compressional waves, and dry Lane Mountain sand packed around them.

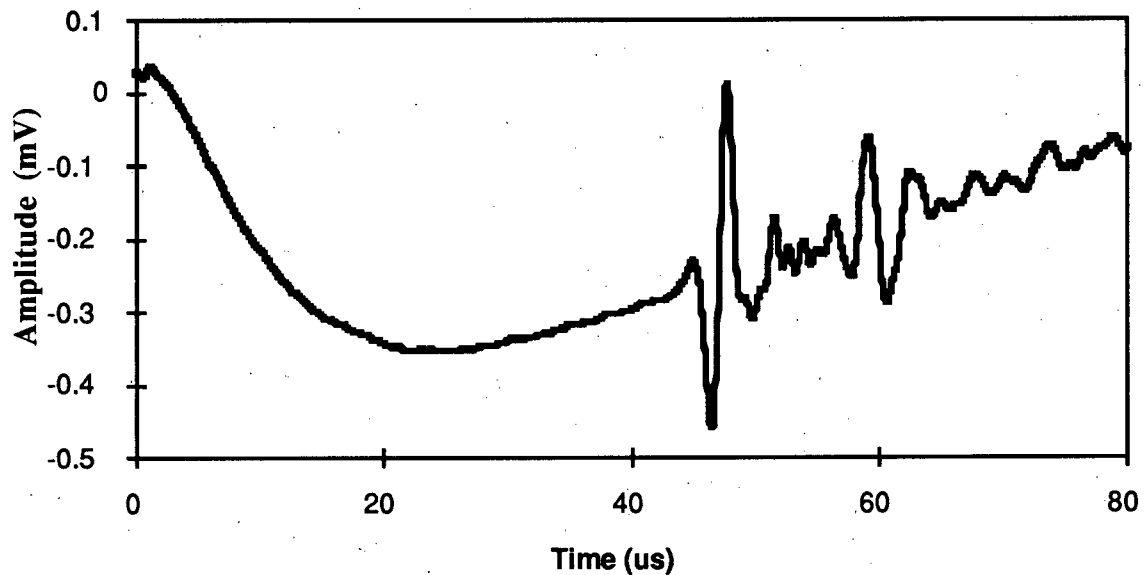


Fig. 3.10b. The received waveform from the confining pressure cell, with benders in an orientation favorable for the propagation of compressional waves, and saturated Lane Mountain sand packed around them.

of the bender electrodes through the saturated sand pack causes the shift of the received waveform.

The data illustrating the measurement of compressional wave velocities in the confining pressure cell are shown in Figure 3.11a. In this figure are shown four different loading cycles of the sand pack, similar to the loading cycles used when the benders were in an orientation favoring shear wave propagation. In Figure 3.11b, the uniaxial strain modulus values are shown, corresponding to the compressional wave velocity measurements. The uniaxial strain modulus M is computed using the formula

$$M = \rho V_p^2 = K + \frac{4}{3}\mu \quad (3.7)$$

where ρ is the density and V_p is the compressional wave velocity. The bulk modulus could not be computed because a reliable estimate of the shear modulus could not be obtained from the sand pack with the benders in a compressional orientation. The dry sand variation in compressional wave velocity and uniaxial strain modulus is very similar to the variation in shear wave velocity and modulus. The cyclic loading of the dry sand pack resulted in a decrease in the uniaxial strain modulus. This can be explained by a reduction in the bulk and shear modulus, due to the increased frictional force near the top of the cell, and the lower confining stress between the bender elements.

After the sand pack was saturated the compressional wave velocity increased to approximately 1700 m/s. Water, which is relatively incompressible, significantly increased the rigidity of the pore spaces. The saturated compressional wave velocity is greater than the velocity of the water alone (~1500 m/s). This was explained by Gassmann (1951) who recognized the contributions of the bulk modulus of the dry sand pack, as well as the bulk modulus of the quartz grains and the bulk modulus of the water to the final bulk modulus of

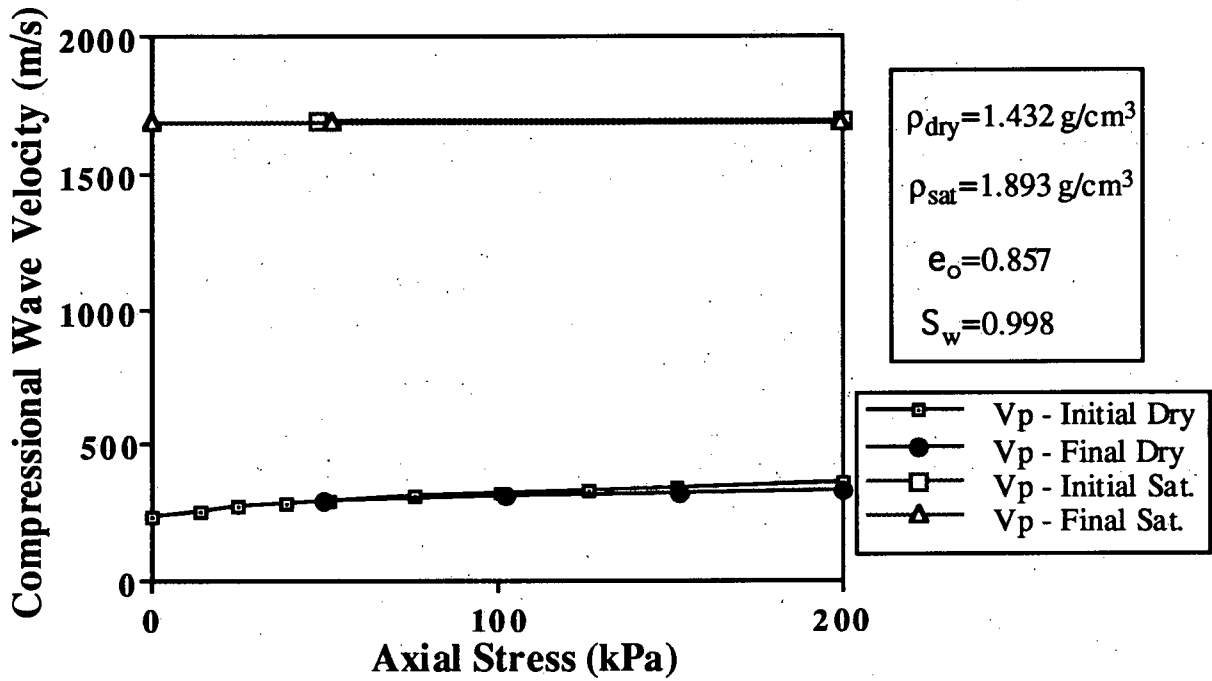


Fig. 3.11a. Compressional wave velocity as a function of confining stress for a dry and water saturated Lane Mountain sand pack.

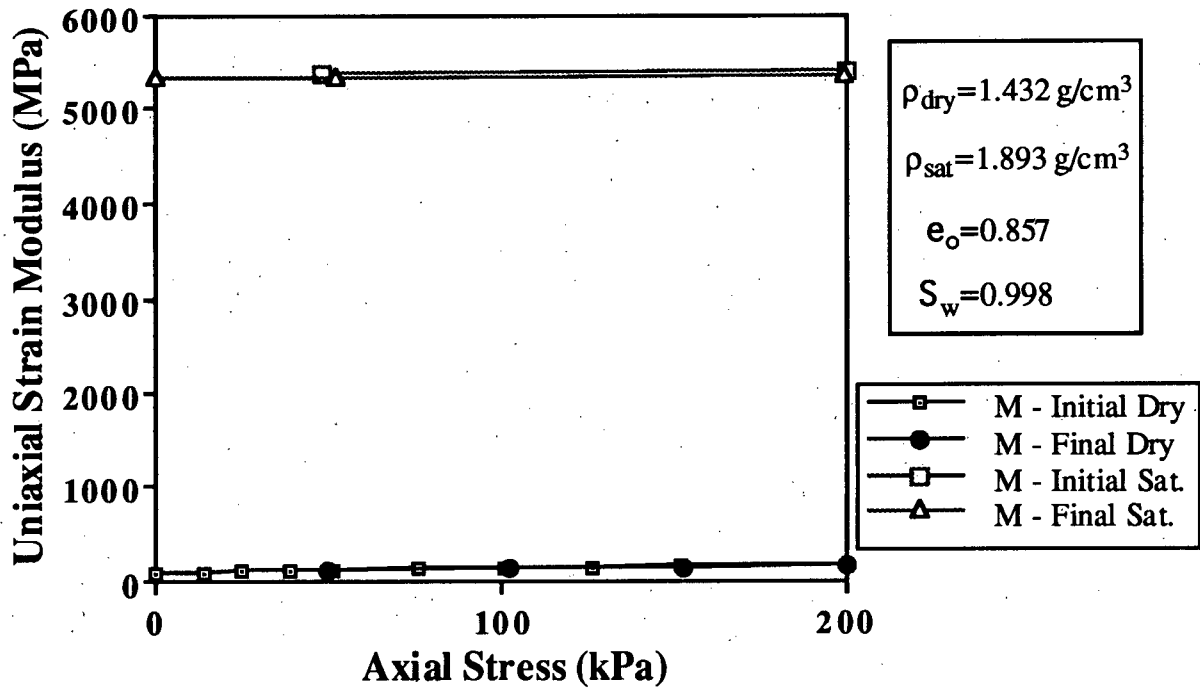


Fig. 3.11b. Uniaxial strain modulus as a function of confining stress for a dry and water saturated Lane Mountain sand pack.

the fully saturated medium. Once saturated, there is no significant variation in compressional wave velocity with axial stress up to 200 kPa. This is similar to the experimental results obtained by Domenico (1977). Domenico found that before saturation the compressional wave velocities increased by the 1/4th power of differential pressure and after saturation the velocity only varied by the 1/18th power of differential pressure. The large change in compressional wave velocity with saturation implies that compressional wave seismic data can be used to differentiate between fully water saturated and partly water saturated sands.

3.6.3 Silicon Oil Saturation Experiments

The purpose of the silicon oil saturation experiments was to test the hypothesis that the pore scale movement of pore fluids, associated with the passage of an elastic wave, is viscosity dependent and will affect the rigidity of a uniform sand pack. It was hypothesized that with increasing viscosity the fluids in the crack-like pore spaces would be less likely to respond to an oscillatory wave. As such they would act in an unrelaxed fashion and increase the rigidity of the sand.

A series of experiments was carried out where the saturating fluid was silicon oil of different viscosities. As shear wave velocity was of primary interest, only the shear wave orientation of the bender elements was used. An example of a bender waveform before and after saturation with silicon oil is shown in Figures 3.12a and 3.12b. The electrical coupling of the benders to the saturated sand pack, apparent in the water saturated case, is not obvious with the silicon oil due to the much lower capacitance of silicon oil compared to water. For each saturation experiment, the modulus varied in a similar fashion, however, there was no systematic change with viscosity to indicate that viscosity has a significant impact on shear modulus. The modulus increased after saturation in almost all cases, but the amount of increase was not systematic with respect to viscosity.

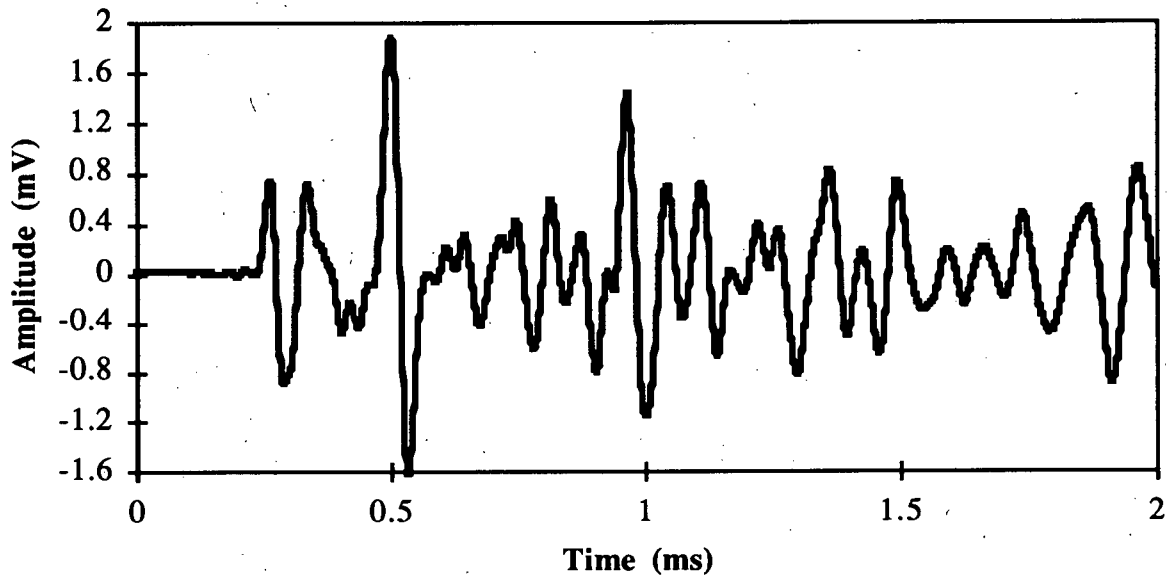


Fig. 3.12a. The received waveform from the confining pressure cell, with benders in an orientation favorable for the propagation of shear waves, and dry Lane Mountain sand packed around them.

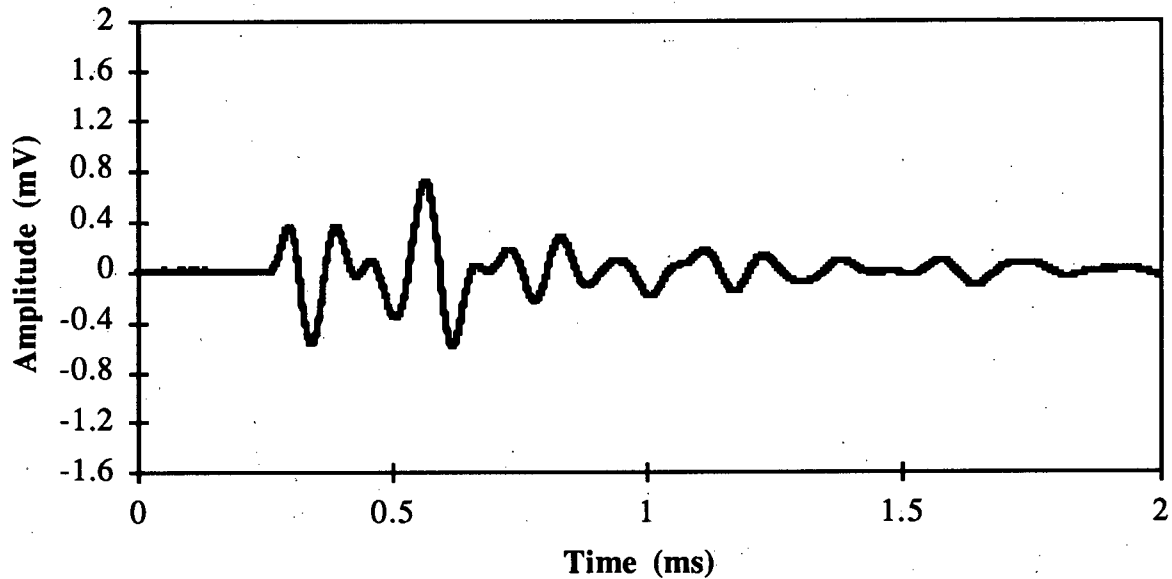


Fig. 3.12b. The received waveform from the confining pressure cell, with benders in an orientation favorable for the propagation of shear waves, and Lane Mountain sand packed around them. The sand from Figure 3.12a is now saturated with 100 mm²/s silicon oil.

3.6.3.1 10 mm²/s Saturation Experiment

The 10 mm²/s silicon oil represents the lowest viscosity used for the saturation experiments. The 10 mm²/s oil has a fluid behavior similar to that of water. The saturation of the sand pack was rapid and the final average saturation was 0.990, with a small air pocket evident at the top of the cell, well away from the bender elements, located at the bottom of the cell. No air bubbles or unsaturated zones were visible within the sand pack. The data show an increase in shear modulus upon saturation, similar to the increase seen with the water saturation experiment.

The 10 mm²/s experiment is shown in Figure 3.13a and in Figure 3.13b, that are graphs showing the variation in shear wave velocity and shear modulus with axial stress. The dry sand loading consisted of a rapid rise in shear modulus up to a confining pressure of 50 kPa, then a slow linear increase to a confining pressure of 200 kPa. The cyclic loading of the sand pack caused a decrease in shear modulus. When the sand was saturated with silicon oil the modulus increased, with the magnitude of the increase changing with confining pressure. After leaving the cell for 2 days the shear wave velocity was again measured with confining pressure ("Final Sat." curve), demonstrating another increase in shear modulus. The sand pack was unloaded and reloaded once again, repeating the "Final Sat." data.

3.6.3.2 100 mm²/s Saturation Experiment

The 100 mm²/s silicon oil saturation experiment represents one of the midrange viscosities with an order of magnitude increase in viscosity compared to the 10 mm²/s experiment. The saturation of the sand pack was slower than the 10 mm²/s experiment, but still relatively rapid. Nitrogen was used to increase the hydraulic head of the silicon oil reservoir. The final saturation of the sand pack was 0.970, with an air pocket evident at the top of the cell. The sand between the benders appeared to be fully saturated. The shear modulus again increased with initial saturation.

The 100 mm²/s saturation experiment is shown in Figure 3.14a and in Figure 3.14b.

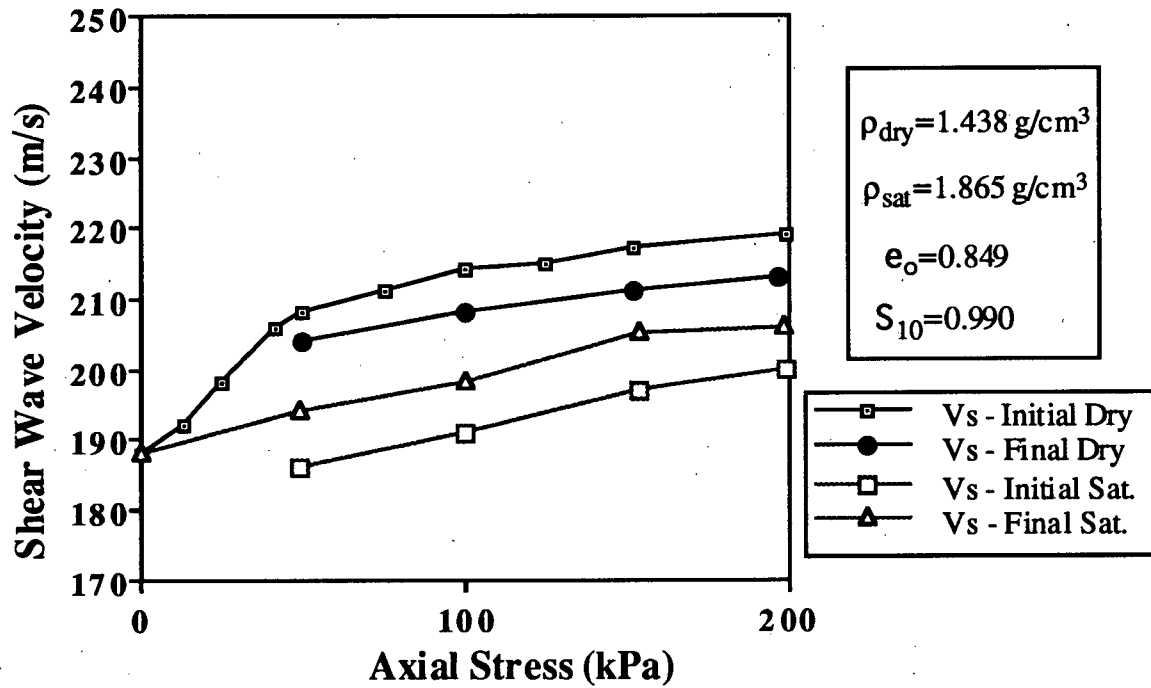


Fig. 3.13a. Shear wave velocity as a function of confining stress for a Lane Mountain sand pack before and after saturation with 10 mm²/s silicon oil.

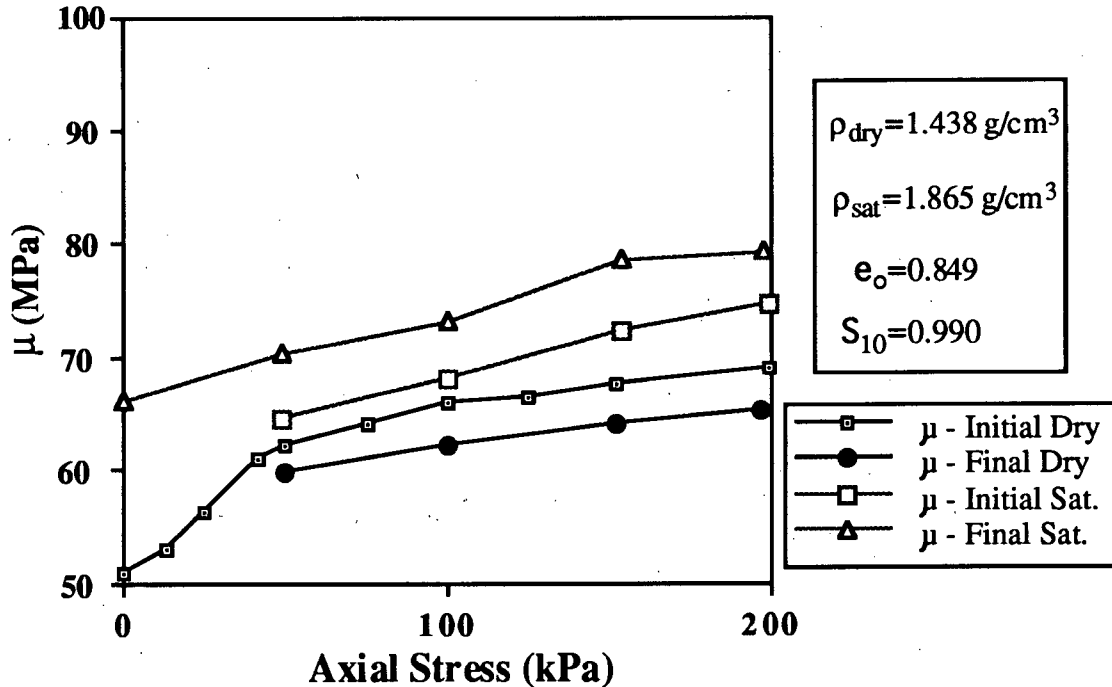


Fig. 3.13b. Shear modulus as a function of confining stress for a Lane Mountain sand pack before and after saturation with 10 mm²/s silicon oil.

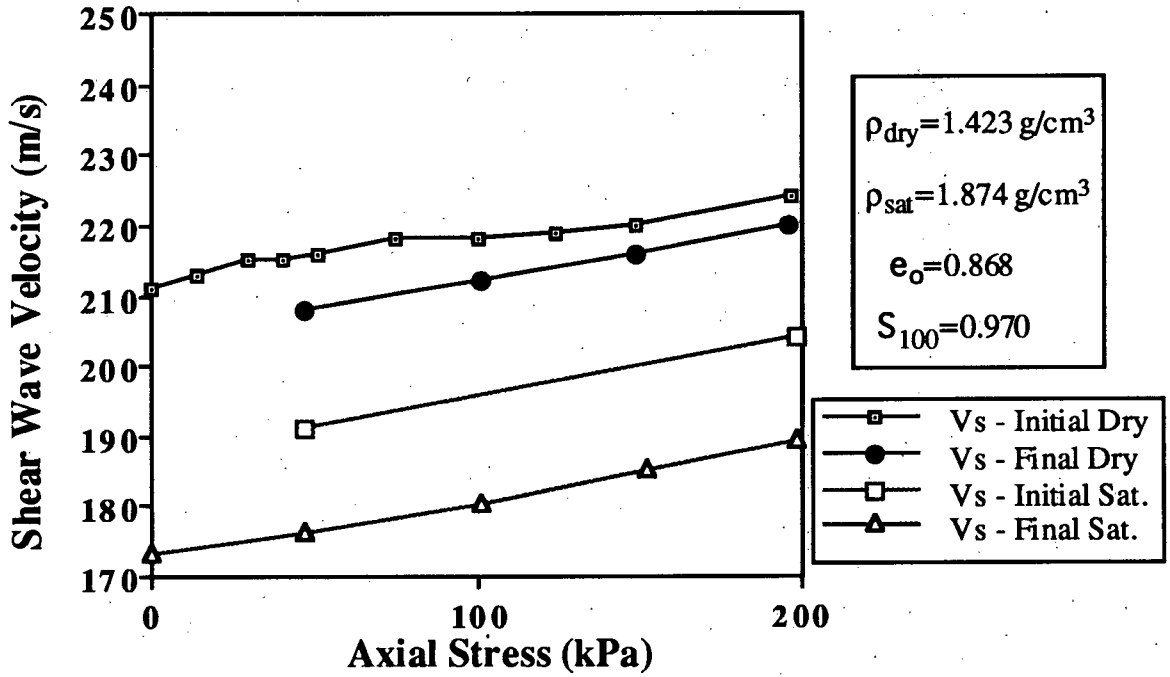


Fig. 3.14a. Shear wave velocity as a function of confining stress for a Lane Mountain sand pack before and after saturation with 100 mm²/s silicon oil.

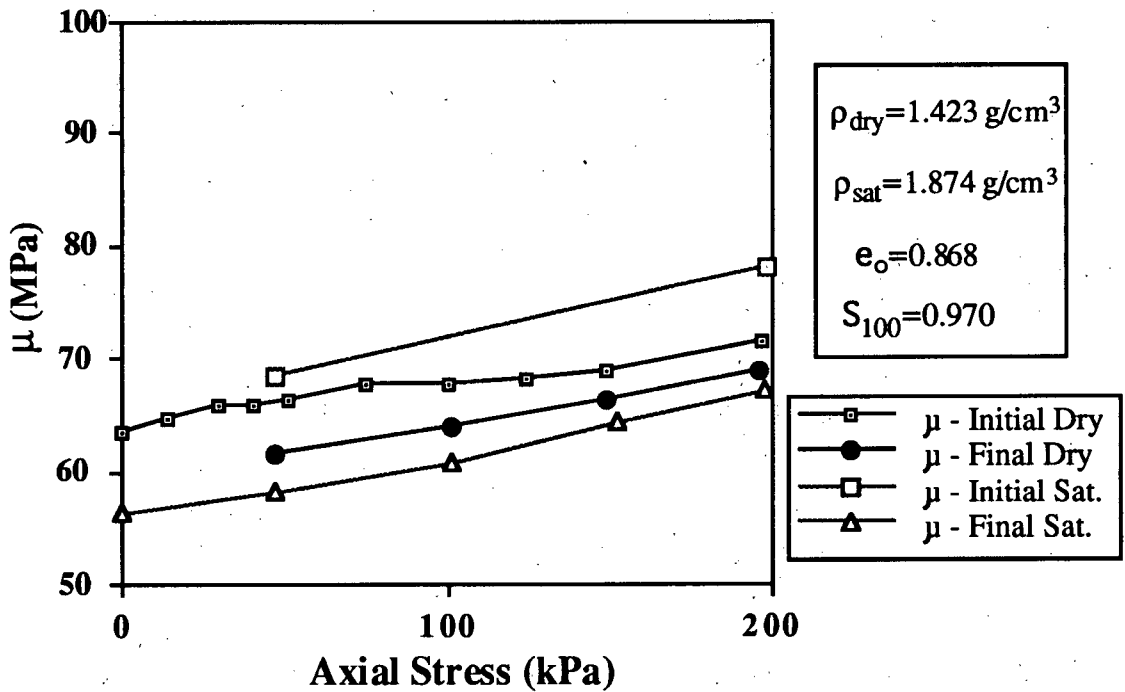


Fig. 3.14b. Shear modulus as a function of confining stress for a Lane Mountain sand pack before and after saturation with 100 mm²/s silicon oil.

The modulus at 200 kPa is similar to the 10 mm²/s experiment, but this time, the loading curve is much straighter, without a significant kink. This is one indication that differences may exist between this sand pack and that used in the 10 mm²/s experiment; such differences can affect the comparison of results. When the sand pack is saturated the shear modulus increases upon initial loading. When the sand pack is left unloaded for 2 days and then reloaded, the modulus is seen to decrease. The modulus decreases so that it is less than all other loading curves. This is the only experiment where this characteristic was observed. The modulus decrease can be explained by an increase in the frictional force or alternatively, the lab temperature may have increased, during the time the sand pack was unloaded.

3.6.3.3 1000 mm²/s Saturation Experiment

The 1000 mm²/s silicon oil saturation experiment represents a further order of magnitude increase in viscosity. The saturation of the sand pack was achieved by applying a 100 kPa head to the silicon oil reservoir. A vacuum was continuously applied to the sand pack while the sand was saturated. It nevertheless required approximately half an hour to saturate the sand. The final saturation was 0.998 with only a small air bubble present above the piston. The data also shows an increase in shear modulus upon saturation.

The 1000 mm²/s experiment is shown in Figure 3.15a and in Figure 3.15b. The dry sand loading is very linear, with only a minor kink perceptible. When the sand was saturated with silicon oil, the modulus increased, with a further increase apparent when the cell was unloaded, left for a day, then reloaded.

3.6.3.4 10 000 mm²/s Saturation Experiment

The 10 000 mm²/s silicon oil represents the highest viscosity fluid that could be used in the apparatus to saturate a sand pack. Even with a 100 kPa head on the silicon oil reservoir, and a vacuum of 30 microns applied, the sand pack required 4 h to fully saturate. The final saturation achieved was 0.994. The data also shows an increase in modulus with

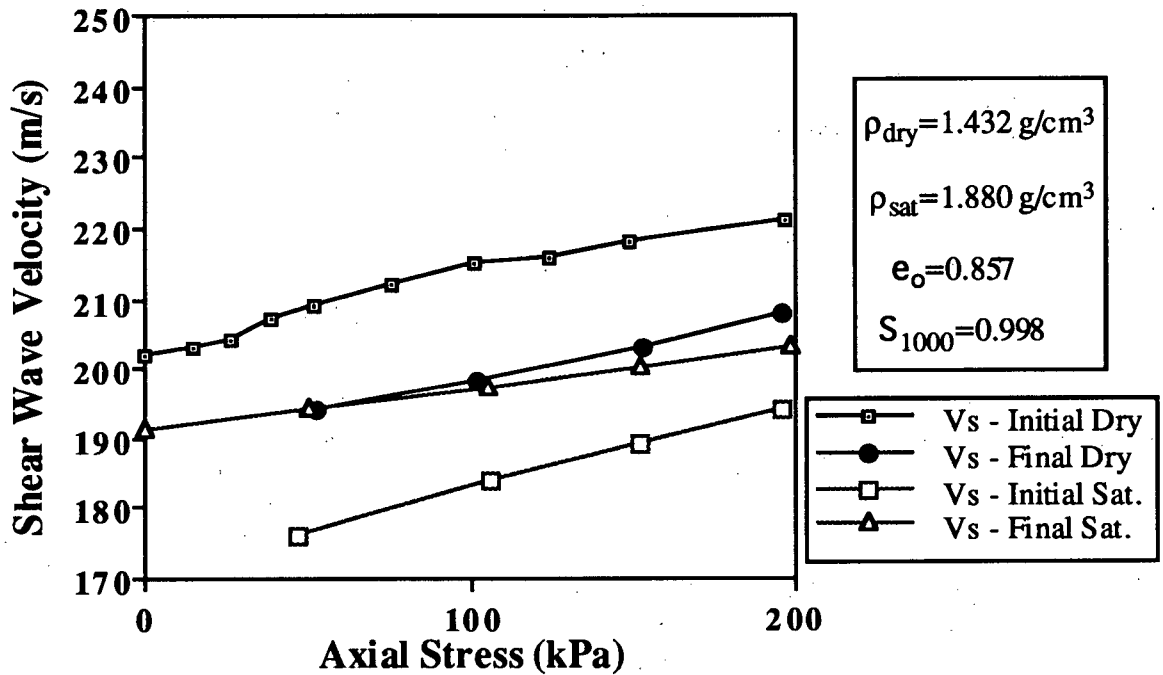


Fig. 3.15a. Shear wave velocity as a function of confining stress for a Lane Mountain sand pack before and after saturation with 1000 mm²/s silicon oil.

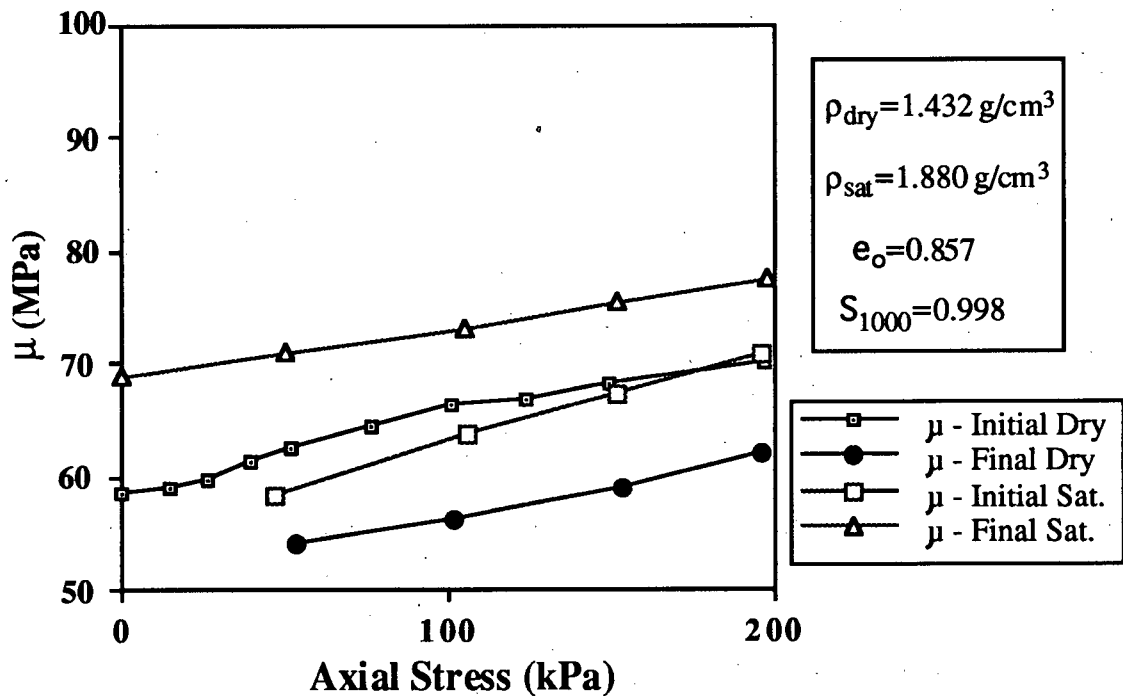


Fig. 3.15b. Shear modulus as a function of confining stress for a Lane Mountain sand pack before and after saturation with 1000 mm²/s silicon oil.

saturation, however, the undrained response of the saturated sand pack played a key role in the results.

The 10 000 mm²/s experiment is shown in Figure 3.16a and in Figure 3.16b. The dry sand loading is very linear, with an initial and final modulus much greater than the other viscosity experiments. The frictional force of the sand on the sides of the cylinder, must be less than in the other experiments, which places the propagating shear waves in a higher confining stress, and increases the shear modulus. When the sand was saturated with silicon oil, the shear modulus increased at the initial axial stress of 50 kPa, which was on the sand pack throughout the saturation process. When the confining stress was increased and maintained for one hour between new readings, the modulus stayed constant. This can be explained by looking at the effective stress.

All the experiments were carried out with the top valve left open while the confining stress was increased. This should result in a drained test, however, in order for the pressure gradients to equilibrate from the increased confining stress, the saturating fluid must flow. With a relatively viscous fluid it will take a significant time for the fluid to flow towards the one point in the cell that is open to atmospheric pressure. This would be most obvious at the highest viscosity. When the load was maintained on the cell overnight, the modulus was found to increase, although it is uncertain whether the fluid pressure had dropped to atmospheric. This highlights the importance of having some type of pressure monitor integrated into the cell in order to determine the fluid pressure and the true effective stress.

3.6.3.5 Discussion of Silicon Oil Experiments

The moduli observed in the different silicon oil experiments, at axial stresses of 50 kPa and 200 kPa, are shown in Figures 3.17 and 3.18. The modulus ratio is defined as the shear modulus after saturation divided by the shear modulus before saturation and is shown in Figures 3.19 and 3.20. The modulus ratio will give an indication of the change in modulus, due to the saturation of the sand. Both the "Initial Dry" and "Final Dry" modulus were used

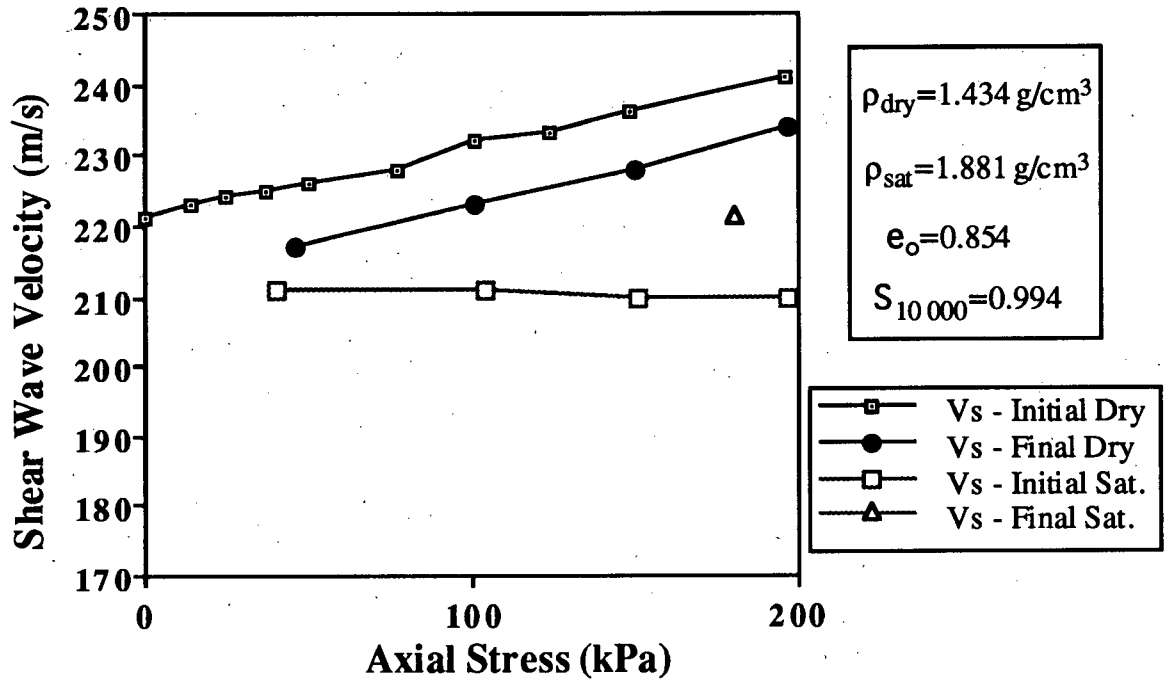


Fig. 3.16a. Shear wave velocity as a function of confining stress for a Lane Mountain sand pack before and after saturation with 10 000 mm²/s silicon oil.

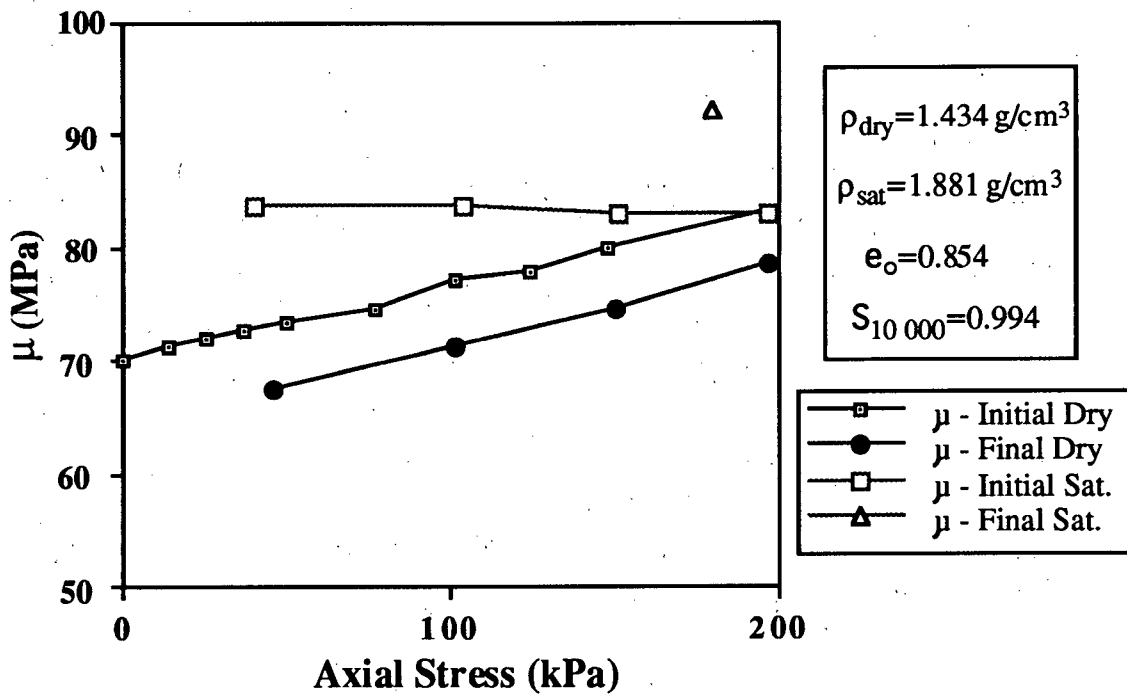


Fig. 3.16b. Shear modulus as a function of confining stress for a Lane Mountain sand pack before and after saturation with 10 000 mm²/s silicon oil.

in the ratios, due to the uncertainty about the affect of the frictional force and how it varies during cyclic loading and saturation. The modulus ratios at both 50 kPa and 200 kPa give no indication of a significant change in shear modulus as a result of the changing viscosity of the saturating fluid. All variations can be explained by changes in stress associated with frictional sliding of the sand along the walls of the Plexiglas cylinder or variations in the lateral stress.

This frictional effect has been recognized by geotechnical engineers in the design of the oedometer device (Lambe and Whitman, 1979). This device also applies a confined compression to a sand pack. The rule of thumb of having a length to diameter ratio of at least 1:3 was adopted, to reduce the effects of side friction. Even with a proper length to diameter ratio, there is no control over lateral stress in the oedometer. This is why most measurements are now made with the triaxial device where complete control over the specimen stress state is possible.

An assumption made in the saturating experiments was that the silicon oil effectively coats the sand grains. A number of experimental procedures, such as the oven-drying of the sand and the pulling of the vacuum were used to reduce the residual water as much as possible, however, it is still possible that a monolayer of water remains attached to the sand grains and prevents the silicon oil from wetting the surface and getting into the smallest crack-like pore spaces. The residual water can be further reduced on future experiments by treating the sand with a fluid such as Quilon-C to make it hydrophobic (Lewis et al., 1988).

The theoretical work of Dvorkin et al. (1994) has not been disproved by the experimental work contained in this thesis. The only way the theoretical analysis will be supported is by performing the experiment in a specially designed triaxial apparatus, that allows the saturation of the specimen by viscous fluids, within the apparatus (not utilized in most triaxial apparatus designs). The lack of a positive result using the bench top Plexiglas cell does illustrate that the variation in shear modulus with viscosity must be quite small. This fact alone, will make it difficult to image lateral changes in viscosity in the field, using shear waves.

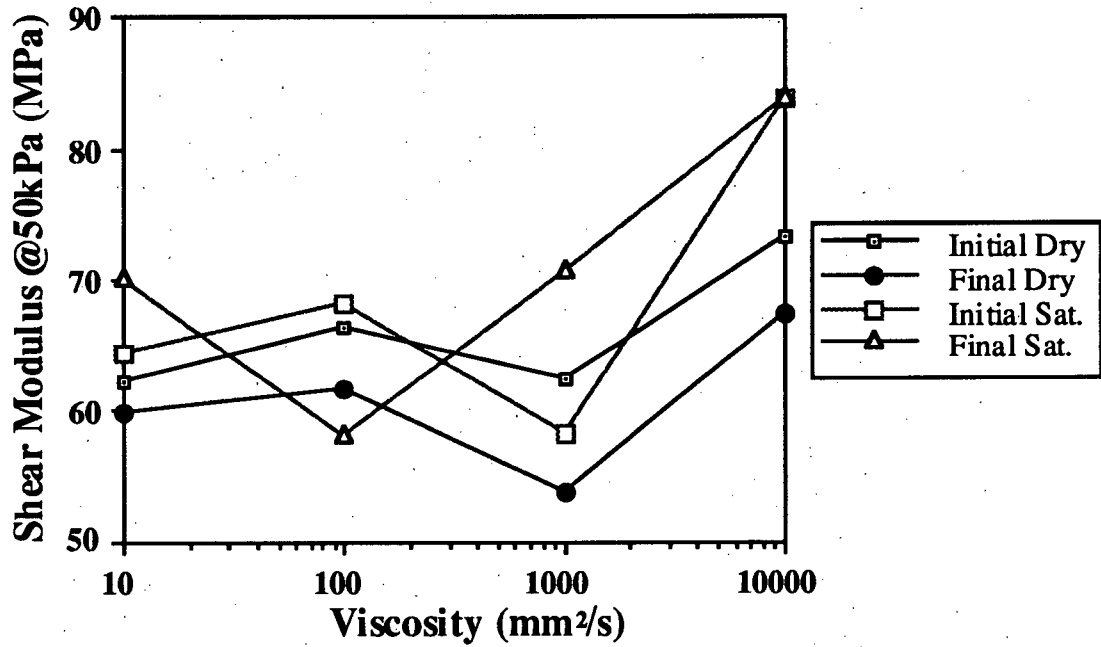


Fig. 3.17. Composite of the shear moduli as a function of viscosity measured at a confining pressure of 50 kPa.

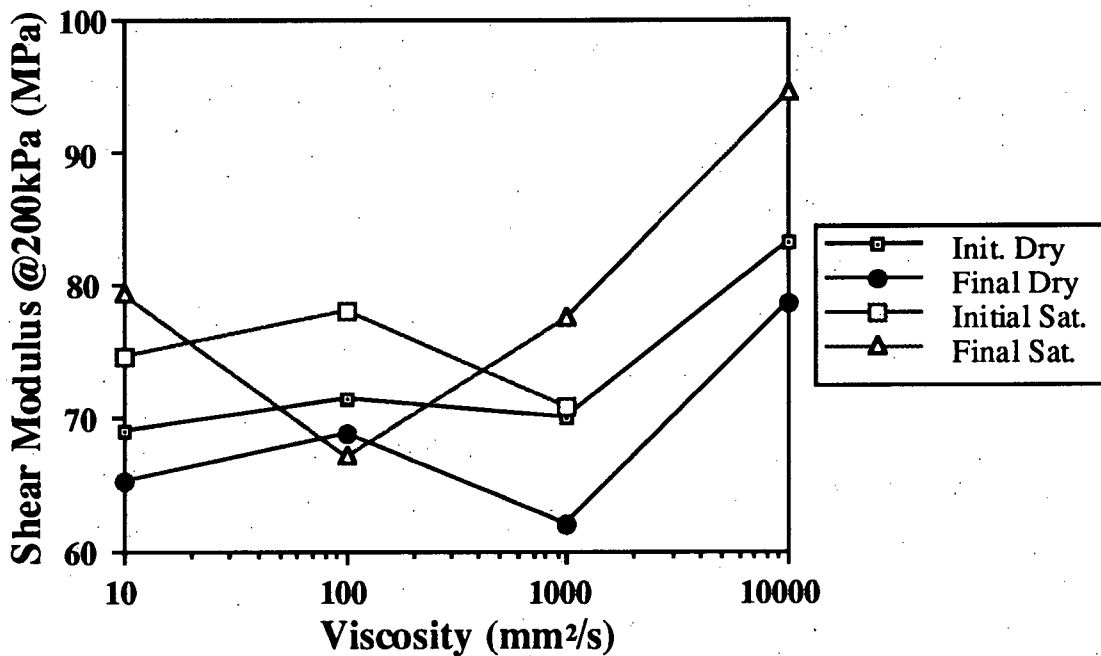


Fig. 3.18. Composite of the shear moduli as a function of viscosity measured at a confining pressure of 200 kPa.

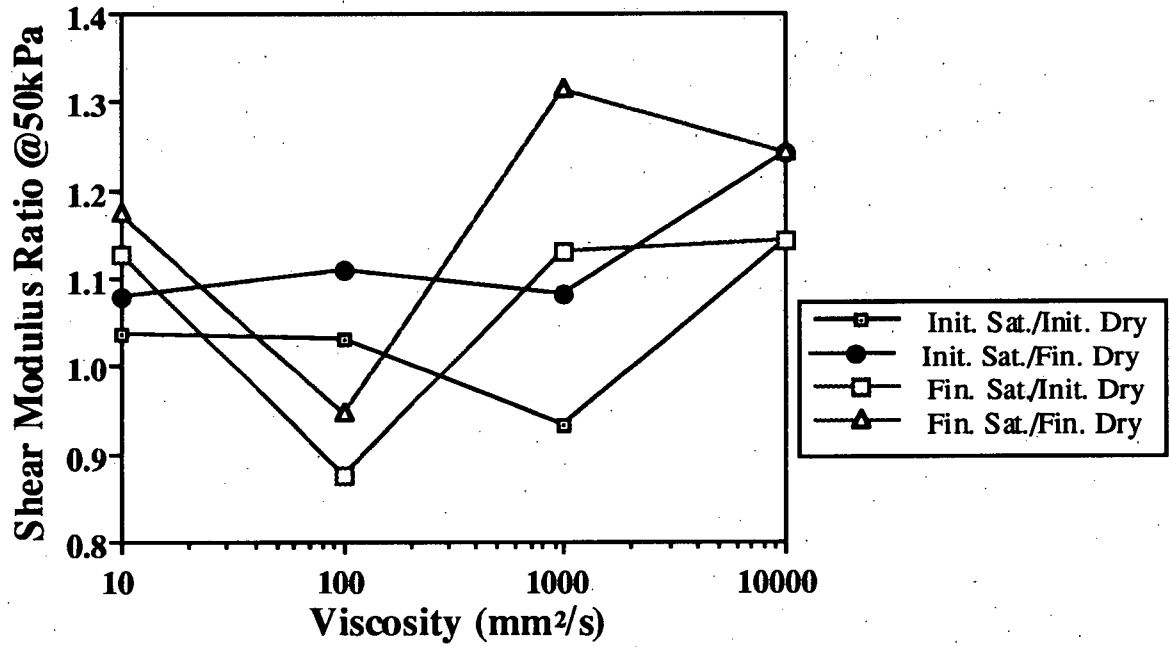


Fig. 3.19. Graph of the shear modulus ratio as a function of viscosity at a confining pressure of 50 kPa.

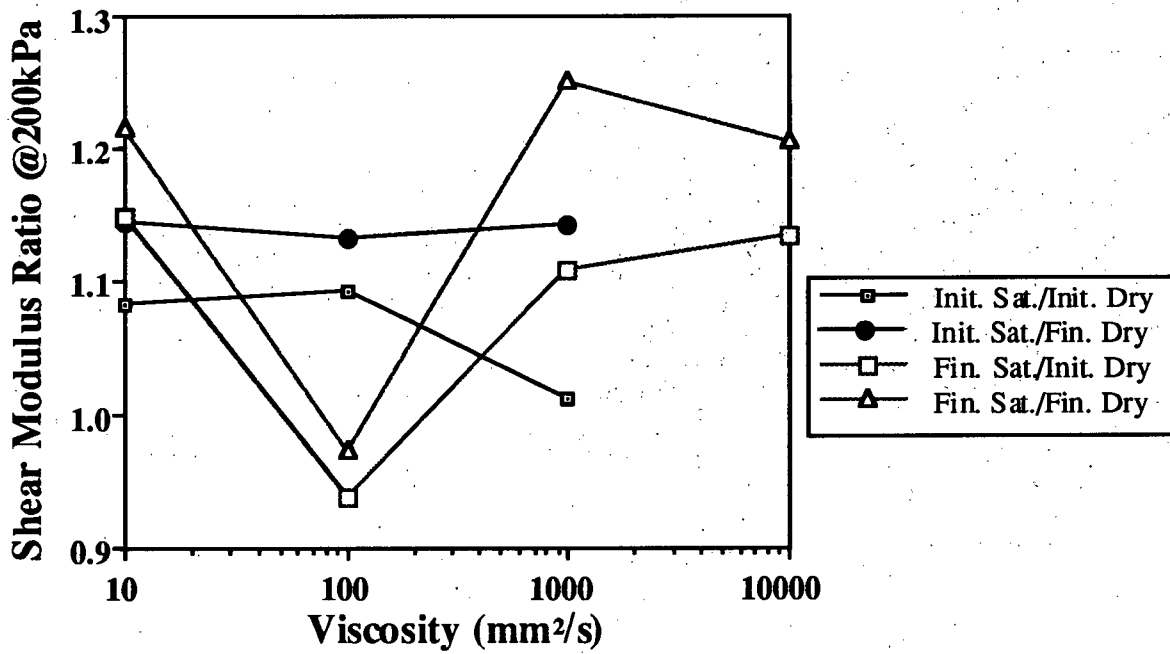


Fig. 3.20. Graph of the shear modulus ratio as a function of viscosity at a confining pressure of 200 kPa.

3.7 Summary

The confining pressure cell with bender elements demonstrated the ability to measure both compressional and shear wave velocities in the laboratory. The shear wave frequencies range from 5 to 15 kHz and the compressional wave frequencies range from 20 to 25 kHz in a dry sand pack to 300 kHz in a saturated sand pack. The first arrival waveform is compact and repeatable from one experiment to the next. A significant limitation of the apparatus was the lack of control over the true confining stress. The variation in stress results from the frictional force of the sand grains on the sides of the cell. Another difficulty is the lack of control over the lateral stress. The lateral stress is generally different from the axial stress under uniaxial compression, which results in an anisotropic stress condition. This anisotropic stress will be highly dependent on the sand packing, causing significant variation in shear wave velocity from one experiment to the next. The variation in shear modulus may in fact be viscosity dependent, however the change is small enough that it is hidden by the variations in the stress state from one experiment to the next. The magnitude of the change is so small it is unlikely to be seen in a field situation where so many other parameters can affect shear wave velocity.

Chapter 4

CONCLUSIONS

The objective of this thesis was to evaluate the application of piezoceramic bender elements to the laboratory measurement of elastic wave velocities. This objective has been met and the bender elements have also shown potential for application to field investigations.

In Chapter 2 the construction of the bender element assembly was discussed. An impedance analyzer was used and proved to be a valuable tool to ensure that the mechanical and electrical response of the two benders was very similar. The benders were inserted into a bucket of dry homogeneous sand to evaluate the characteristic waveforms associated with the propagation of both compressional and shear waves. The shear waveform was compact with minor compressional wave interference and demonstrated the broadband response of the elements. The compressional waveform did show some shear wave interference, which occurred after the first arrival. This makes the use of the benders, as currently configured, inadequate for the generation of purely compressional impulses. They can still be used for first arrival measurements, however, to obtain the compressional wave velocity of a cohesionless material. The accurate measurement of velocities in cohesionless material was the subject of Chapter 3.

In Chapter 3 the bender element assemblies were inserted in a confining pressure cell to make measurements of both shear and compressional wave velocities in a cohesionless sand pack. The Plexiglas cell enabled both the variation in confining stress and the saturation of a sand pack with both water and silicon oil. The cell demonstrated that the benders were well suited to the measurement of elastic wave velocities. The received waveform was characterized by a large amplitude early arrival that made the picking of first breaks unambiguous. Variations in confining stress within the cell between experiments made repeatable measurements of velocity difficult. The shortcomings of the cell result from the

uniaxial stress state of the cell and the frictional force of the sand along the sides of the cell. This frictional force varied between experiments, resulting in a variation of the stress state. The variation in stress state had a significant impact on the both the bulk and shear modulus and hence the elastic wave velocities. As a result of the variation in confining stress, an experiment using the cell to examine the dependence of the shear modulus on the viscosity of the saturating fluid was inconclusive. The bender element assembly was built to fit in the confines of a Plexiglas cylinder, which has an inside diameter of 8 cm, with a versatile mounting design that can be used in other laboratory apparatus. This includes the insertion in a steam flood apparatus (Butler, 1994) to measure the changes in elastic wave velocity during a laboratory steam flood.

The application to field investigations was demonstrated by the sand bucket and sandbox experiments. The short compact shear waveform generated was visible, above the noise, for a distance of 35 cm. For the bender elements utilized, with a driving voltage of 3 V, a separation of 15 to 20 cm was the most realistic for making accurate measurements of the average velocity of a sand/silt mixture. Larger separations are possible if larger input voltages are used. The benders are extremely well suited to cohesionless material; this implies they can be used as probes for making in situ velocity measurements. The short compact shear waveform also shows significant promise for using the benders for shallow seismic reflection imaging applications.

REFERENCES

- Becker, G.E., 1990, Velocity of sound in various media, *in* Lide, D.R., Ed., CRC Handbook of Chemistry and Physics, 71st Edition: CRC Press, 14-32.
- Butler, D.B., 1994, The electrical nature of subsurface steam flow: Rock Physics Research Program Annual Report, University of British Columbia, 3, G1-G14.
- De Alba, P., Baldwin, K., Janoo, V., Roe, G., and Celikkol, B., 1984, Elastic wave velocities and liquefaction potential: Geotechnical Testing Journal, 7, 77-87.
- Domenico, S.N., 1977, Elastic properties of unconsolidated porous sand reservoirs: Geophysics, 42, 1339-1368.
- Dvorkin, J., Yin, H., and Knight R., 1994, Seismic detection of residual contaminants: 64th Ann. Internat. Mtg., Soc. Expl. Geophys., Expanded Abstracts, 584-586.
- Dyvik, R. and Madshus, C., 1985, Lab measurements of G_{max} using bender elements: Advances in the Art of Testing Soils Under Cyclic Conditions Conference, Detroit, MI, Geotechnical Engineering Division, ASCE, Expanded Abstracts, 185-196.
- Dyvik, R. and Olsen, T.S., 1989, G_{max} measured in oedometer and DSS tests using bender elements: 12th Intl. Conf. on Soil Mech. and Foundation Eng, Rio de Janero, Vol 1.
- Gassmann, F., 1951, Uber die elastizitat poroser medien: Veir der Natur Gesellscheft, 96, 1091-1098.
- Goertz, D., 1994, An experimental study of the effects of partial saturation on elastic wave velocities in porous rocks: M.Sc. thesis, University of British Columbia.
- Gohl, W. B., 1990, Response of pile foundations to simulated earthquake loading: experimental and analytical results: Ph.D. thesis, University of British Columbia.
- Hughes, D.S. and Cross, J.H., 1951, Elastic wave velocities in rock at high pressures and temperatures: Geophysics, 16, 577-593.
- Lambe, T.W. and Whitman, R.V., 1979, Soil Mechanics, SI Version: John Wiley & Sons.

- Lewis, M.G., Sharma, M.M., and Dunlap, H.F., 1988, Effect of overburden pressure and the nature of the microscopic distribution of fluids on electrical properties of rocks: Trans. SPWLA 29th Synp., K1-K11.
- Mavko, G. and Jizba, D., 1991, Estimating grain-scale fluid effects in velocity dispersion in rocks: *Geophysics*, **56**, 1940-1949.
- Mavko, G., and Nur, A., 1979, Wave attenuation in partially saturated rocks: *Geophysics*, **44**, 161-178.
- O'Connell, R., and Budiansky, B., 1974, Seismic velocities in dry and saturated cracked solids: *J. Geophys. Res.*, **79**, 5412-5426.
- O'Connell, R., and Budiansky, B., 1977, Viscoelastic properties of fluid-saturated cracked solids: *J. Geophys. Res.*, **82**, 5719-5736.
- Shirley, D.J., 1978, An improved shear wave transducer: *J. Acoust. Soc. Am.*, **63**, 1643-1645.
- Shirley, D.J. and Hampton, L.D., 1978, Shear-wave measurements in laboratory sediments: *J. Acoust. Soc. Am.*, **63**, 607-613.
- Taylor, J.R., 1982, *An Introduction to Error Analysis: University Science Books*, 52-59.
- Terzaghi, K., 1923, Die berechnung der durchlassigkeitsziffer des tones aus dem verlauf der hydrodynamischen spannungserscheinungen: *Sitz. Akad. Wissen. Wien Math-naturw Kl. Abt. IIa*, **132**, 105-124.
- Thomann, T.G., and Hryciw, R.D., 1990, Laboratory measurement of small strain shear modulus under K_0 conditions: *Geotechnical Testing Journal*, **13**, 97-105.
- Yan, L., 1990, Hydraulic gradient similitude method for geotechnical modelling tests with emphasis on laterally loaded piles: Ph.D. thesis, University of British Columbia.
- Yu, P., Richart, F.E., 1984, Stress ratio effects on shear modulus of dry sands: *Journal of Geotechnical Engineering*, **110**, 331-345.